MARMARA UNIVERSITY

INSTITUTE FOR GRADUATE STUDIES

IN PURE AND APPLIED SCIENCES

STRUCTURAL DYNAMICS OF VON HIPPEL-LINDAU TUMOR SUPRESSOR PROTEIN

TANDAÇ FÜRKAN GÜÇLÜ

M.Sc. THESIS

Department of Bioengineering

ADVISOR

Assist. Prof. Dr. A. NEVRA ÖZER

ISTANBUL, 2015

MARMARA UNIVERSITY

INSTITUTE FOR GRADUATE STUDIES

IN PURE AND APPLIED SCIENCES

STRUCTURAL DYNAMICS OF VON HIPPEL-LINDAU TUMOR SUPRESSOR PROTEIN

TANDAÇ FÜRKAN GÜÇLÜ

524213002

M.Sc. THESIS

Department of Bioengineering

ADVISOR

Assist. Prof. Dr. A. NEVRA ÖZER

ISTANBUL, 2015

MARMARA UNIVERSITY
INSTITUTE FOR GRADUATE STUDIES IN PURE AND APPLIED SCIENCES

Tandaç Fürkan GÜÇLÜ, a Master of Science student of Marmara University Institute for Graduate Studies in Pure and Applied Sciences, defended his thesis entitled "STRUCTURAL DYNAMICS OF VON HIPPEL-LINDAU TUMOR SUPPRESSOR PROTEIN", on ....., 2015 and has been found to be satisfactory by the jury members.

Jury Members

Assist. Prof. Dr. A. Nevra ÖZER (Advisor)
Marmara University .....(SIGN).....

Assist. Prof. Dr. Pemra ÖZBEK SARICA (Jury Member)
Marmara University .....(SIGN).....

Assist. Prof. Dr. Özge KÜRKÇÜOĞLU LEVİTAS (Jury Member)
Istanbul Technical University .....(SIGN).....

APPROVAL

Marmara University Institute for Graduate Studies in Pure and Applied Sciences Executive Committee approves that Tandaç Fürkan GÜÇLÜ be granted the degree of Master of Science in Department of Bioengineering, Bioengineering Program on 03.07.2015 2015. (Resolution no: 2015/14-02

Director of the Institute

Prof. Dr. Uğur YAHŞİ

ACKNOWLEDGEMENTS

The work presented in this thesis was conducted in the Computational Biology and Bioinformatics Laboratory at the Bioengineering Department of Marmara University which was established by the financial support of BAPKO in the framework of the Infrastructure Project No. FEN-E-300409-0119.

I would like to express my gratitude to my thesis supervisor Assist. Prof. Dr. A. Nevra ÖZER for her continuous guidance, generous support, and valuable advice and for being a pleasure to work with.

İSTANBUL, JUNE 2015 **Tandaç Fürkan GÜÇLÜ**

CONTENTS

ÖZET

VON HIPPEL-LINDAU TÜMÖR BASKILAYICI PROTEİNİNİN YAPISAL DİNAMİĞİ

Böbrek kanseri dahil birçok organda selim ve habis tümör oluşumuyla nitelenen kalıtsal otozomal dominant bir hastalık olan von Hippel-Lindau (VHL) kanser sendromu, von Hippel-Lindau tümör baskılayıcı proteini (pVHL) üzerindeki mutasyonlarla ilişkilidir. Elongin C-Elongin B bileşiğine bağlı bulunan pVHL üzerindeki mutasyon, hipoksiyle indüklenebilir faktör (HIF) ve vasküler endotelyal büyüme faktörü (VEGF) üretimini aktive ederek tümör oluşumuna yol açar. Bu çalışmada, bilgisayar ortamında tasarlanan Elongin C ve HIF zincirlerine bağlı pVHL yapısı, Moleküler Dinamik (MD) simülasyon metodu kullanılarak simüle edilmiş ve elde edilen yapılardan veri kümeleme metodu ile temsilci yapılar seçilerek yapısal dinamik analizlerinde kullanılmıştır. Bileşiğin yaban tipi ve tasarlanmış Y98N, Y98N-G123F ve Y98N-D179N mutant yapılarının dinamiği, proteinlerde normal modlara dayalı üç boyutlu harmonik titreşimsel analiz yaparak kollektif hareketlerinin yönlerini ve boyutlarını tahmin eden Eşyönsüz Ağyapı Modeli (ANM) ile karşılaştırmalı olarak incelenmiştir. Rezidülerin dalgalanma yönleri, özellikle hareket boyutları en düşük olan ve dinamik olarak önemli dayanak bölgelerinin etrafında değişiklik göstermektedir. Bu da, proteinlerde dayanak bölgelerinin dinamik davranış biçiminin işlevle ilişkili olduğunu ispatlamaktadır. ANM ile hesaplanan en kooperatif işlevsel hareket modlarında protein rezidülerindeki dalgalanma yönleri ve dalgalanmalar arasındaki korelasyonların analizi sonucunda, yaban tipi dinamik davranış biçiminin Y98N mutant yapınınkine kıyasla Y98N-G123F mutant yapısınınkine benzer olduğu gösterilmiştir. Y98N-D179N çiftli mutant yapısında ise, Y98N mutantından sapmalar ve yaban tipine benzerlikler daha çok dalgalanmalar arasındaki korelasyonlarlarda belirgindir. Bu sonuçlar, hastalıkla alakalı proteine eklenen ikinci mutasyonlarla yaban tipi dinamiği ve işlevinin geri kazanıldığını göstermektedir. Genel olarak bu çalışma, pVHL sistemindeki moleküler etkileşimlerin ve evrimsel optimizasyonun yapısal dinamik temellerini açıklayarak VHL hastalığına yönelik ilaç tasarımı çalışmalarına yardımcı olacaktır.

ABSTRACT

STRUCTURAL DYNAMICS OF VON HIPPEL-LINDAU TUMOR SUPPRESSOR PROTEIN

The von Hippel-Lindau (VHL) cancer syndrome is associated with mutations on the von Hippel-Lindau tumor suppressor protein (pVHL), which activates the production of the hypoxia inducible factor (HIF) and the vascular endothelial growth factor (VEGF) leading to tumor growth. In this work, the mutant structures of the pVHL bound to Elongin C and HIF which were built in silico were relaxed by Molecular Dynamics (MD) simulations and the representative members of the MD trajectories generated by clustering were submitted to further computational structural dynamics analysis. The dynamics of wild-type, tumor-related Y98N mutant, and Y98N-G123F and Y98N-D179N double mutant complex structures were assessed comparatively utilizing the Anisotropic Network Model (ANM). The directions of fluctuations differ mainly around the important hinge regions in the minima of the most cooperative mode shapes, justifying that the dynamic nature of hinges should correlate with the functioning of proteins. The analyses of orientation of fluctuations and correlations between fluctuations in the functional modes of ANM indicate that the dynamic behavior of the Y98N-G123F double mutant is similar to that of the wild-type compared to the Y98N mutant which is known to be associated with the VHL disease. However, in the Y98N-D179N double mutant structure, deviation from Y98N mutant and accordance with wild-type is observed mostly in the correlations between fluctuations. These results indicate a regain of wild-type dynamics, and thus wild-type function, with the addition of the second mutations to the disease-related variant. Overall, this study would help in the drug design studies for the VHL disease by explaining molecular recognition and evolutionary optimization in the pVHL system from a structural dynamics perspective.

LIST OF SYMBOLS

α	Alpha
β	Beta
Å	Angstrom

LIST OF ABBREVATIONS

ANM	Anisotropic Network Model
GNM	Gaussian Network Model
HIF	Hypoxia Inducible Factor
MD	Molecular Dynamics
NMA	Normal Mode Analysis
PCA	Principal Component Analysis
pVHL	von Hippel-Lindau protein
RMSD	Root Mean Square Deviation
VCB	pVHL-Elongin C-Elongin B
VEGF	Vascular Endothelial Growth Factor
VHL	von Hippel-Lindau

LIST OF FIGURES

LIST OF TABLES

CHAPTER 1 AIM OF THE STUDY

The reason behind the constant increase in the incidence of kidney cancer has not been clarified yet [1] and the molecular biology and pathology of this disease is highly related with the VHL tumor suppressor gene and its protein pVHL [2]. pVHL is a marginally stable tumor suppressor protein and the mutation on the pVHL bound to the Elongin C-Elongin B complex activates the production of the hypoxia inducible factor (HIF) and the vascular endothelial growth factor (VEGF) which in turn leads to tumor growth [3]. Yet there are few studies on the correlated allosteric effects between binding sites, on the relationship between interdomain linkage and disease-related mutations, and on pVHL instability and design of stable pVHL structures [4].

In this thesis, mutant structures of the pVHL bound to Elongin C and HIF, which had been experimentally demonstrated to have variable stabilities and binding affinities [4], were built in silico for further computational structural dynamics analysis. The dynamics of the wild-type, the designed Y98N mutant, the designed Y98N-G123F double mutant, and the designed Y98N-D179N double mutant complex structures were studied by the Anisotropic Network Model (ANM) [5] based on normal modes analysis (NMA). The comparative detailed analyses of the residue fluctuations in the most cooperative functional modes of the ANM demonstrate the loss and regain of wild-type function of the pVHL system as a result of the mutations on the protein. Overall, this work is aimed to contribute in the drug design studies for the VHL disease by explaining the molecular recognition and evolutionary optimization in the pVHL system from a structural dynamics perpective.

CHAPTER 2 INTRODUCTION

2.1 VHL disease

VHL disease is a neoplastic, autosomal, dominant and hereditary disease that leads to growth of tumors like renal cell carcinoma, retinal and central nervous system haemangioblastomas, phaeochromocytomas and pancreatic neuroendocrine tumors, also pancreatic and renal cysts [2]. Eye-related symptoms of the VHL disease were revealed in 1894 by Treacher Collins [6]. The term VHL disease was used in 1936 which arises from the first description of angiomas in retina by Eugen von Hippel in 1904 and spinal and cerebellar tumors by Arvid Lindau in 1927, and the name of VHL has been in common use since around 1970 [7]. Differential diagnosis procedure is introduced in 1964 that permitted the treatment of the VHL disease in patients that have whether tumors or familial history of VHL disease [7].

Biochemical studies displayed that pVHL structure forms a three-domain complex with the transcription elongation factors C and B, and the term VCB has been used since mid-1990s [8], [9]. This protein domains are important for the pVHL function, and aminoacid construction of Elongin C and Elongin B were determined in 1999 [3]. In the mid-1990s it was observed that vascular tumors related with the VHL disease lead to overproduction of angiogenic proteins like VEGF [10].

The initial biochemical finding that pVHL may have a significant factor in the transduction of signals originated by differences in environment oxygen pressure described in 1996 [11]; cell carcinoma in kidney cells with inadequate wild-type pVHL protein level were observed to produce mRNAs for VEGF synthesis and platelet-derived growth factor subunit B under both hypoxic and normoxic conditions. When the wild-type but not the mutant pVHL is inserted into these cells with specifically inhibited production of these mRNAs under normoxic conditions, the cells should restore their previous metabolic states [12].

2.2 VHL gene and protein pVHL

From a genetics point of view, the von Hippel–Lindau disease demonstrates an autosomal dominant pattern of inheritance. Linkage analysis of mapped VHL-related

genes showed that the VHL gene is in the locus of chromosome 3p25 [13]. A germline mutation of VHL was displayed in essentially all patients who have a diagnosis of VHL disease. In up to 20% of VHL patients there is complete loss of either the paternal or the maternal VHL locus. Tumorigenesis that due to VHL disease is highly related to inactivation or loss of the remaining wild-type VHL allele [14].

The VHL disease is highly related with the mutations on the von Hippel-Lindau tumor suppressor protein which function has been investigated entirely [1], [15]. pVHL binds to Elongin C and Elongin B, and then inhibits the hypoxia-inducible factor (HIF) under normoxic conditions. The HIF heterodimer, which is formed by the loss of pVHL or in hypoxic conditions, binds to specific DNA sequences. Then, transcription of some hypoxia-inducible genes, like VEGF which induces vascularization and tumor growth, is activated.

pVHL structure consists of two coupled domains, α and β, where the β-domain consists of two β-sheets arranged with an α-helix on top [16]. The α-domain directly contacts Elongin C and the β-domain interacts with HIF [16]. pVHL is stabilized by associating with Elongin C, whereas Elongin B and Elongin C are stabilized through their interactions with each other and with pVHL [17]. All domains of VCB complex are thus resistant to degradation by proteasome [18]. On the other hand, pVHL mutations that cause deformation of Elongin binding are unstable and the mutant proteins are rapidly degraded by the proteasome [19].

2.3 Tumor-related mutations on pVHL

Previous experimental and computational studies showed that VCB complex has a significant role in tumor suppression function and most of the tumor-related mutations destabilize this complex [4], [20]–[24]. Additionally, peptide mapping studies revealed that the mutated regions of pVHL make important interactions with Elongin C, presenting the Elongin C binding and tumor suppression functions of pVHL [3], [17]. The Y98N mutant which leads to cell carcinoma in kidneys was shown to be less stable and the affinity of binding with HIF is less than that of the wild-type pVHL, indicating that there is a correlation between binding affinity and stability of pVHL and HIF [4]. Yet when the stabilizing mutations, G123F and D179N, were inserted into the Y98N

tumor-related mutant pVHL and the structures were analyzed by molecular dynamics (MD) simulations, it was observed that these substitutions stabilized the Y98N mutant and its binding interface to HIF [18], [23]. That is, the mutations G123F and D179N could lead the tumor-related mutant pVHL to improve its stability and thus regain its wild-type function apparently. The studies in literature showed that both thermodynamic properties and dynamic allosteric factors between domains of the VCB complex were determined by the interaction sites [4], [23]–[25]. Thus, the drugs that mimic the mutants in terms of allosteric effects might reverse the function of pVHL to gain a more stable state in the VHL disease.

2.4 Structural Dynamics Analyses

Important dynamic and functional properties can be enlightened by extensive analyses of fluctuations of biomolecular complexes [26]. Biological function is highly correlated with the cooperative modes of motion with greater amplitude [25]. These modes with low frequency are extracted by decomposing the dynamics into modes of motion [27]. The principal component analysis (PCA) is a statistical procedure that uses the fluctuations calculated in molecular dynamics (MD) trajectories and deduces collective behavior [28]. As an alternative, the cooperative dynamics can be evaluated by normal modes analysis (NMA) [29], [30]. Elastic network models based on NMA are computationally simple methods that have been well accepted in recent years to assess the large scale cooperative motions of proteins [26], [27], [31], [32]. They are introduced by the work of Tirion [33] where a uniform harmonic potential model is used to represent the vibrational properties of macromolecules. The applications of the elastic network models such as the Gaussian Network Model (GNM) [34], [35] and the Anisotropic Network Model (ANM) [5] have produced significant results that are accordant with those of Molecular Dynamics (MD) simulations and experimental studies [36]–[38]. Essentially, the motion of hinge residues examined by the ANM has shown to be a critical inducing factor for functional dynamics of macromolecules [39]. The fluctuations of these flexible hinge areas activate the correlated fluctuations of large domains effectively. These central hubs determine the intrinsic dynamics of the protein structure [40].

In this work, the effect of sequence variations on the stability of the pVHL system was studied using a mechanistic functional dynamics perspective. To this end, MD simulations were performed on wild-type, in silico designed tumor-related Y98N mutant, in silico designed Y98N-G123F double mutant and in silico designed Y98N-D179N double mutant pVHL structures bound to Elongin C and HIF. Clustering was carried out on each trajectory to gather MD-relaxed snapshots which represent the dynamic features of the trajectories. Then, the representative structures obtained by clustering were analyzed with the ANM and the intrinsic dynamics of functionally important regions that govern the conformational ensembles of pVHL variants were investigated.

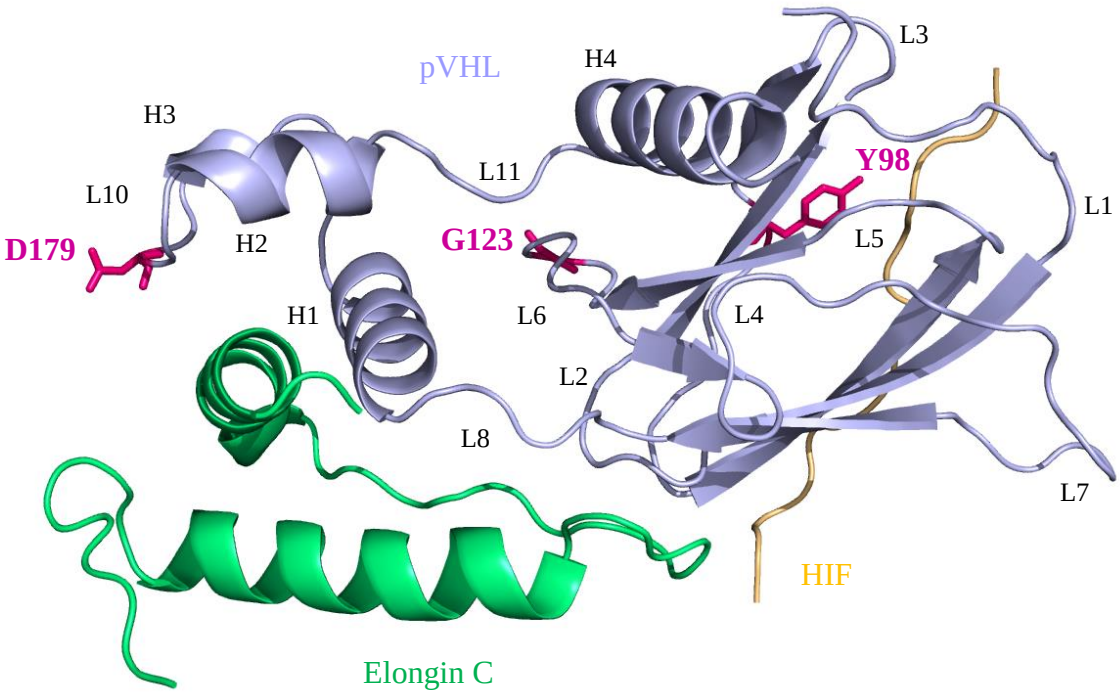

Figure 2.1 Crystal structure of the Elongin C-pVHL-HIF complex (PDB identifier 1LM8). pVHL is shown in purple, Elongin C is shown in green and HIF is shown in orange. The important loops and helices on the pVHL chain are labeled. The tumor-related (Y98) and designed (G123, D179) mutant residues are shown in magenta.

CHAPTER 3 MATERIALS AND METHODS

3.1 Structures

The crystal structure of pVHL bound to Elongin B, Elongin C and HIF (PDB identifier 1LM8) was used by excluding Elongin B as it is 25Å far from the Elongin C-pVHL-HIF interaction sites and the direct effect of Elongin B on the related interdomain sites is insignificant and irrelevant for this study. Also on the Elongin C chain, since the coordinates for residues 49-57 were unavailable and residues 17-48 were distant from the pVHL-Elongin C binding site, residues 17-57 were completely excluded. Using this crystal structure as a model template, the Y98N, the Y98N-G123F, and the Y98N-D179N mutant protein structures were built with the Mutator plug-in of the VMD [41] software.

3.2 Molecular Dynamics simulations and Clustering

MD simulations were first developed to investigate chemical reactions and the quantum-mechanical motions of large molecular systems in the late 1970s [42]. To reduce the complexity of computation and simulate the atomic dynamical behavior, MD simulation method is established based on Newtonian physics [43]. The schematic of simulation process is illustrated in Figure 3.1, where a structural model of a protein structure is gathered from X-ray crystallographic or magnetic resonance data at the first step. Then, the forces from bonded and non-bonded interactions are calculated. The bonded interactions such as atomic angles, chemical bonds, dihedral angles and the non-bonded forces that arise due to van der Waals interactions are modeled by using Lennard-Jones potential and electrostatic interactions using the Coulomb's law. In order to simulate the actual behavior of real molecules in motion, the energy terms are parameterized to fit experimental data and quantum-mechanical calculations. These combined parameters are defined as force fields, which describe the various atomic forces that govern the molecular dynamics. Once the forces from the initial state of the atoms in the system are calculated, the positions of these atoms are changed according to the Newton's law of motion.

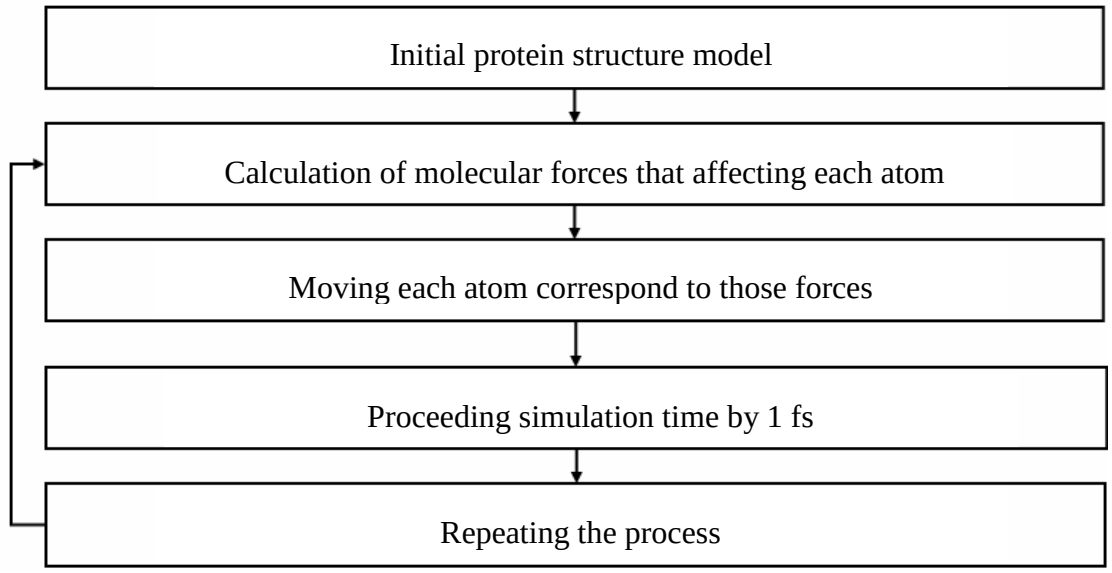

Figure 3.1 A schematic diagram showing the Molecular Dynamics simulation process

In this study, MD simulations were performed with NAMD [44], by using the CHARMM22 force field [45]. The wild-type and mutant structures were solvated in a TIP3P water box with a minimum distance of 10 Å from each atom. The total charge of the system was neutralized with sodium or chloride atoms. The whole system was minimized for 10000 steps by using the steepest descent algorithm. The simulations were carried out for 20 ns at 310 K constant temperature. Temperature was controlled by using Langevin Dynamics. Nosé-Hoover Langevin piston pressure control was used as a barostat to keep the system at 1 atm constant pressure.

Conformations of the wild-type, Y98N, Y98N-G123F and Y98N-D179N protein structures were generated by MD simulations of 20 ns. Then, the snapshots obtained within the first 5 ns of each trajectory, which consist of the non-equilibrium state, were eliminated to gather more stable structures. To select the dynamically essential conformations of the 15 ns long MD simulation trajectories, the snapshots within the production phase were clustered separately. The MMTSB toolset [46] was used to perform k-means clustering which is based on root-mean-square deviation (RMSD) between conformations as the mutual similarity measure. The RMSD cutoff denotes the radius of a cluster, which is the maximum atomic distance between all the protein structures in the cluster and the cluster centroid. Here, 15,000 snapshots for each 20 ns

MD trajectory were clustered by using 1.5 Å RMSD cutoff. Then, the largest clusters' representatives were selected for further ANM analysis.

3.3 Anisotropic Network Model

ANM [5] performs a harmonic vibrational analysis to predict both the magnitudes and also the directionalities of the motions of macromolecular structures around their states in equilibrium. The neighboring heavy atoms are connected to form the elastic network and then the conformations that depict the residue fluctuations from their mean positions in the principal directions of motion are produced. For a system of N nodes, the total potential energy consists of all harmonic interactions of adjunt *(i, j)* pairs computed as:

$$V = (\gamma / 2)\left[\sum_{i,j}^{N} h(r_c - R_{ij})(R_{ij} - R_{ij}^{\,0})^2\right] \tag{3.1}$$

$R_{ij}^{\,0}$ is the equilibrium distance and R_{ij} is the instantaneous distance between sites *i* and *j* in the native structure. γ is the harmonic force constant. $h(r_c\text{-}R_{ij})$ is the Heaviside step function that is zero if $(r_c\text{-}R_{ij}) < 0$ and 1 otherwise. r_c is the cutoff distance that was taken as 9 Å in this study.

The Hessian matrix *H* is constructed, which is a *3Nx3N* symmetric matrix that carries the anisotropic data about the directionality of nodes *i* and *j*. There are *NxN* superelements H_{ij} in this matrix of second derivatives of the potential *V*, each of size *3x3*. The normal modes of the elastic network are obtained by the orthogonal transformation of the real symmetric Hessian matrix, with *3N-6* nonzero eigenvalues λ_i and corresponding eigenvectors u_i.

$$H^{-1} = \sum_{i=1}^{3N-6} \frac{1}{\lambda_i} u_i u_i^T \tag{3.2}$$

The pairs of alternative conformations sampled by the individual modes are built and viewed explicitly by the fluctuation vectors, simply by adding them to the equilibrium position vectors. The distribution of mobility among the residues is revealed by the mode shapes in different frequency modes.

The cross-correlation between the fluctuations of sites *i* and *j* is calculated as:

$$\langle \Delta R_i . \Delta R_j \rangle = \left(3k_B T / \gamma \right) tr\left[H^{-1} \right]_{ij} \tag{3.3}$$

where $tr[H^{-1}]_{ij}$ is the trace of the ij^{th} submatrix $[H^{-1}]_{ij}$ of H^{-1}. When $i=j$, the self-correlations between the components ΔR_i are obtained.

The orientational correlations between two different protein structures are determined by calculating the dot product of the fluctuation vectors. Then, the cosine values between the vectors are assessed after the structures are superimposed. The normalized correlation values vary between 1 and -1. The perfect correlation with value of 1 refers to 0° angle, and the maximum variation in direction with correlation value of -1 refers to 180° angle of the fluctuation vectors of the aligned structures. The residues that exhibit lower orientational correlation values correspond to the regions with increased variations in their directions of motion. Here, the orientational correlations of each of the residues were evaluated in the two slowest modes of motion to investigate the directional variation between wild-type and mutant pVHL complex structures [47].

CHAPTER 4 RESULTS AND DISCUSSION

The dynamics of the wild-type crystal structure and the in silico designed mutant structures of the pVHL complex were analyzed by a structure-based method. The structures were first simulated by MD and then clustered to obtain representative conformations of the trajectories. Then, using an elastic network model, namely the ANM, the size and orientation of motion of residues in the pVHL system were elaborated comparatively between different complex structures.

4.1 Representative conformations of pVHL variants

The wild-type and the in silico designed Y98N, Y98N-G123F and Y98N-D179N mutant structures of pVHL complex were simulated by MD to generate minimized and relaxed conformations. Different from previous computational studies of pVHL, the human body temperature 310 K was used as constant temperature in the simulations. The simulations were carried out for 20 ns, where the RMSD values of the wild type and mutant structures' trajectories indicate that each equilibrium state was achieved after 5 ns (Fig.4.1). Thus, the conformations of the first 5 ns in non-equilibrium state were excluded for the clustering analysis. Then, 15,000 MD-generated conformations for each pVHL complex structure were clustered by an RMSD measure where the cluster radius was set to 1.5 Å.

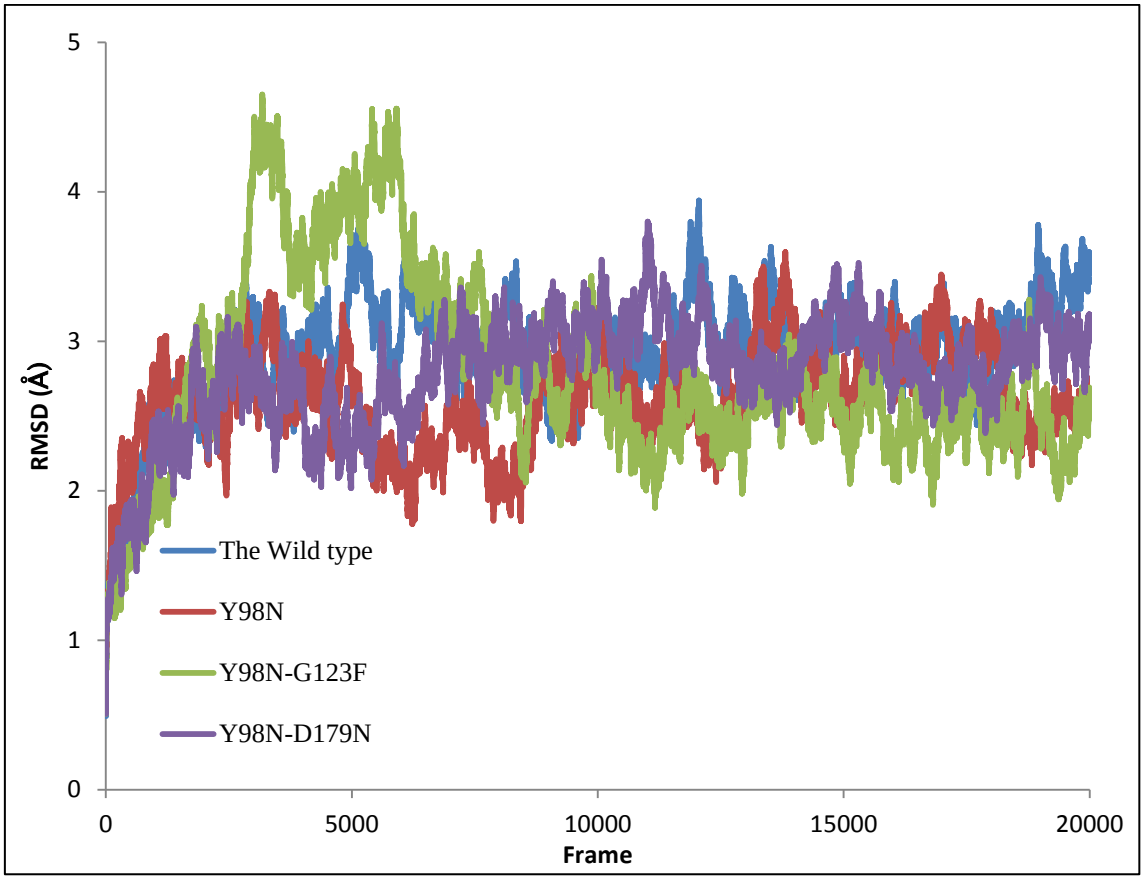

Figure 4.1 The RMSD of Elongin C-pVHL-HIF complex for the wild-type (blue), in silico designed tumor-related mutant Y98N (red), in silico designed double mutant Y98N-G123F (green) and in silico designed double mutant Y98N-D179N (purple).

Various RMSD cutoff radius values were tried in order to achieve optimum precision and convergence in the clustering procedure. Since convergence of MD simulations might not be reached by even long trajectories, the convergence here was decided by the relative proportions of the clusters [48]. When the RMSD cutoff value was increased, low number of clusters with low precision was obtained. A value of RMSD cutoff with high precision was determined by the evaluation of the number of distant and irrelevant snapshots in the clusters. Since MD simulation is a time-dependent deterministic method, adjacent snapshots in a trajectory are not expected to present drastically different dynamic behavior. Further, the dynamic behavior of those adjacent snapshots in the same cluster should be correlated with the RMSD pattern of the whole trajectory. Additionally, it was observed that outliers from different clusters occupied the largest

cluster when the RMSD cutoff was increased, leading to a decrease in precision of the clustering as well.

The cluster percentages with RMSD cutoff values of 1.5 Å, 1.8 Å and 2.0 Å are given on Tables 4.1-3 respectively. When the RMSD cutoff was set to 1.5 Å, the trajectories of wild-type, Y98N mutant, Y98N-G123F double mutant and Y98N-D179N double mutant have 5, 11, 12 and 6 clusters, where the percentages of the largest clusters are 31%, 16%, 18% and 28% respectively (Table 4.1). The trajectory of the Y98N-G123F double mutant structure has the highest number of clusters, which indicates that it has the greatest mobility compared to the other structures. On the other hand, the trajectory of the Y98N mutant has the second highest number of clusters and the lowest cluster percentage compared to the other structures. Also, the cluster percentages of the Y98N mutant have very close values. Therefore, it is clear that the Y98N mutant has both high mobility and more number of substates with 1.5 Å cutoff, which exhibits that this structure has lower dynamic stability compared to the other structures. The clusters obtained with RMSD cutoff values of 1.8 Å and 2.0 Å were also tested by performing the ANM on the best members of largest clusters and the results were exceedingly different between cluster members.

Table 4.1 Cluster percentages of MD-sampled structures with 1.5 Å RMSD cutoff

	Wild-type	Y98N	Y98N-G123F	Y98N-D179N
Cluster 1	31	16	18	28
Cluster 2	19	13	10	22
Cluster 3	18	13	10	17
Cluster 4	17	12	9	13
Cluster 5	16	10	9	12
Cluster 6		10	8	8
Cluster 7		8	8	
Cluster 8		6	7	
Cluster 9		5	7	
Cluster 10		4	7	
Cluster 11		2	5	
Cluster 12			4	

Table 4.2 Cluster percentages of MD-sampled structures with 1.8 Å RMSD cutoff

	Wild-type	Y98N	Y98N-G123F	Y98N-D179N
Cluster 1	72	19	30	42
Cluster 2	28	18	18	31
Cluster 3		17	12	26
Cluster 4		16	12	
Cluster 5		14	11	
Cluster 6		14	8	
Cluster 7		2	8	

Table 4.3 Clusters percentages of MD-sampled structures with 2.0 Å RMSD cutoff

	Wild-type	Y98N	Y98N-G123F	Y98N-D179N
Cluster 1	73	28	30	100
Cluster 2	27	22	21	
Cluster 3		18	19	
Cluster 4		17	18	
Cluster 5		15	11	

The representative conformations of each of the trajectories were chosen from the largest clusters as the structures with the minimum distance from the cluster centroids. The second distant structures and the second largest clusters in each trajectory were also considered, yet the second distant structures showed highly similar results to the representative structures while second largest clusters showed highly different and inconsistent ANM results between cluster members. The structures of the representative

conformations from largest clusters that were further analyzed by the ANM (Figure 4.2) show that the Y98N-G123F and the Y98N-D179N double mutant structures have similar conformations, whereas the Y98N tumor-related mutant conformation has differences in structure. Similarity measure is assessed by calculating the RMSD by backbone with the wild type complex as reference structure. The RMSD values are 1.3, 0.8, 0.8 for the Y98N mutant, the Y98N-G123F double mutant and the Y98N-D179N double mutant structures, respectively.

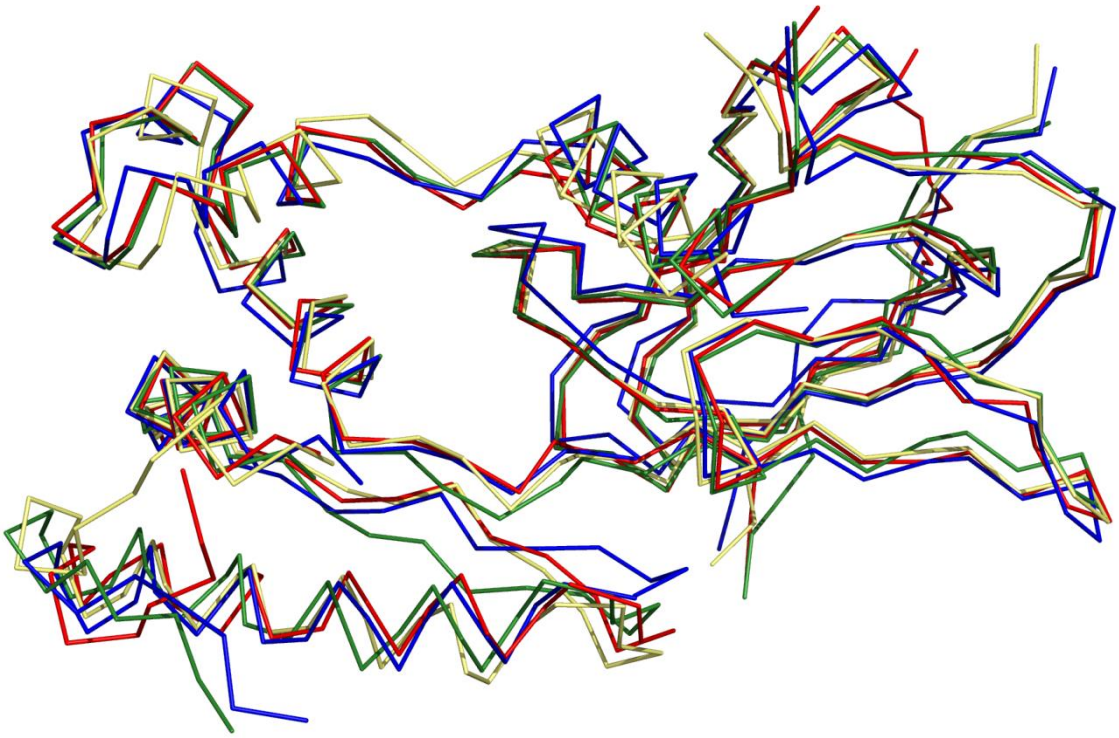

Figure 4.2 Representative structures of Elongin C-pVHL-HIF complex from each MD trajectory. The wild-type is shown in red, the Y98N mutant is shown in blue, the Y98N-G123F double mutant is shown in green and the Y98N-D179N double mutant is shown in yellow.

4.2 Motion and residue fluctuations in principal directions

The mechanisms of the cooperative molecular motions relevant to function are implied by the low frequency modes of motion [49]. Here, the motion of the wild-type and mutant pVHL structures in the cooperative low frequency modes were comparatively analyzed with the ANM. The fluctuations in the principal directions refer to the main

functional motion of the structures and the collective modes of motion are highly robust against sequence and structure variations. Thus, all pVHL complex structures that are functional should display similar modes of motion.

The contributions of the three most cooperative functional modes to the overall motion are 18%, 14% and 7%, respectively, as calculated over the first 50 modes of the wild-type structure with the frequency of the following modes decaying rapidly.

As a representative structure, the motions of the wild-type Elongin C-pVHL-HIF complex structure in the slowest three modes are displayed on Figures 4.3-5 respectively. In these most cooperative modes of motion, large scale movements are observed at the loops at the surface regions of both Elongin C and pVHL chains. The residues within the core regions and the interaction sites are less mobile as their motion is restricted as a result of binding. In the first mode (Figure 4.3), both Elongin C and pVHL chains fluctuate parallel to the *y* direction. H1 helix and L8 loop of pVHL chain are less mobile compared to H3 helix and L3 loop of pVHL chain due to binding. In the second mode (Figure 4.4), H1 helix and L2, L6, L8 loops of pVHL chain are less mobile compared to H4 helix and L3, L1 loops of pVHL chain. The overall movement of the pVHL chain is parallel to *z* direction. In the third mode (Figure 4.5), H1 helix and L5 loop is less mobile compared to the mobile L2, L6 and L8 loops. The pVHL chain rotates around the *y*-axis, N-terminus displays parallel movement to the *x* axis and L6, L1, L7 loops move parallel to *z* axis.

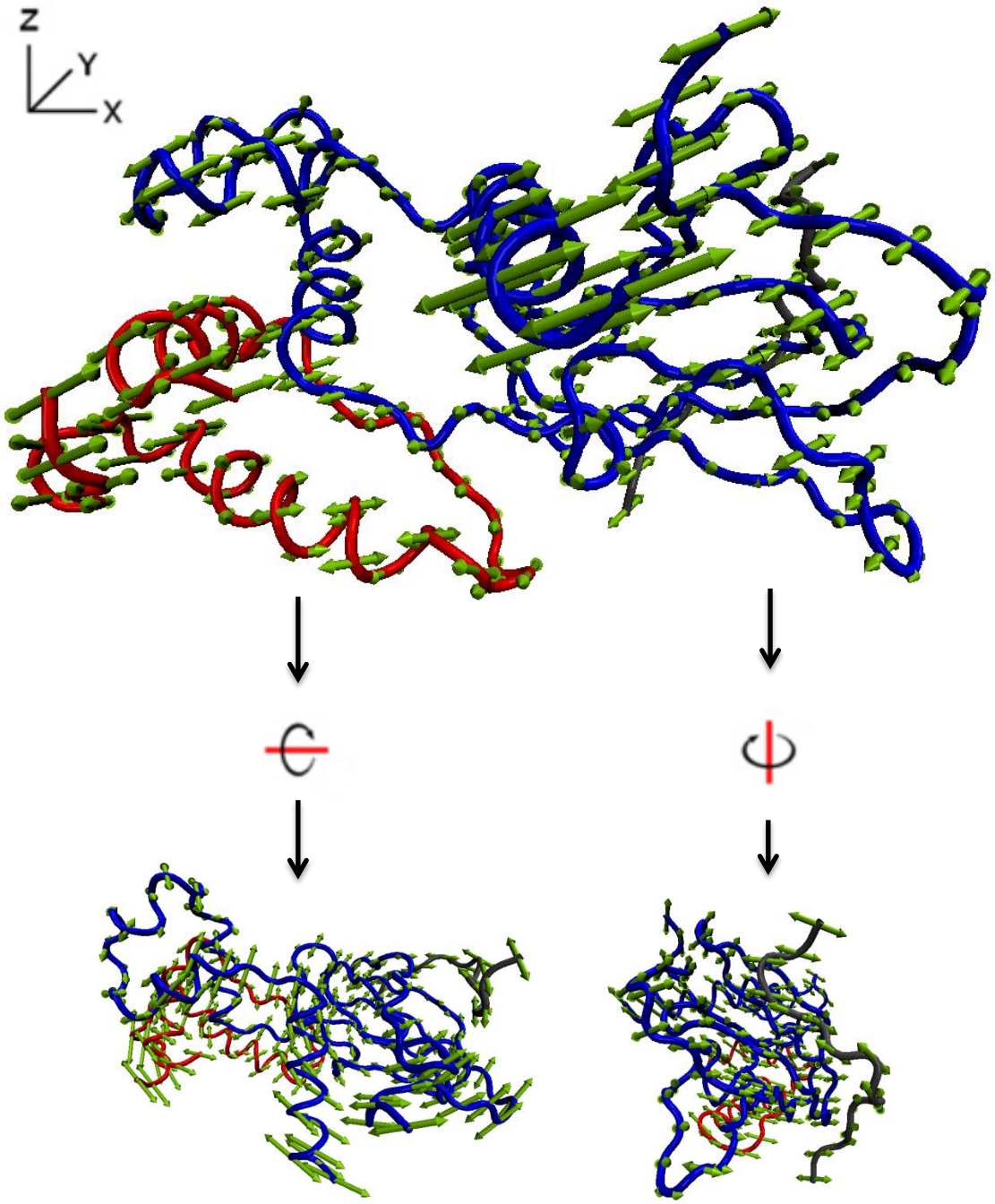

Figure 4.3 Motion of Elongin C-pVHL-HIF complex in the slowest mode. pVHL is shown in blue, Elongin C is shown in red and HIF is shown in grey.

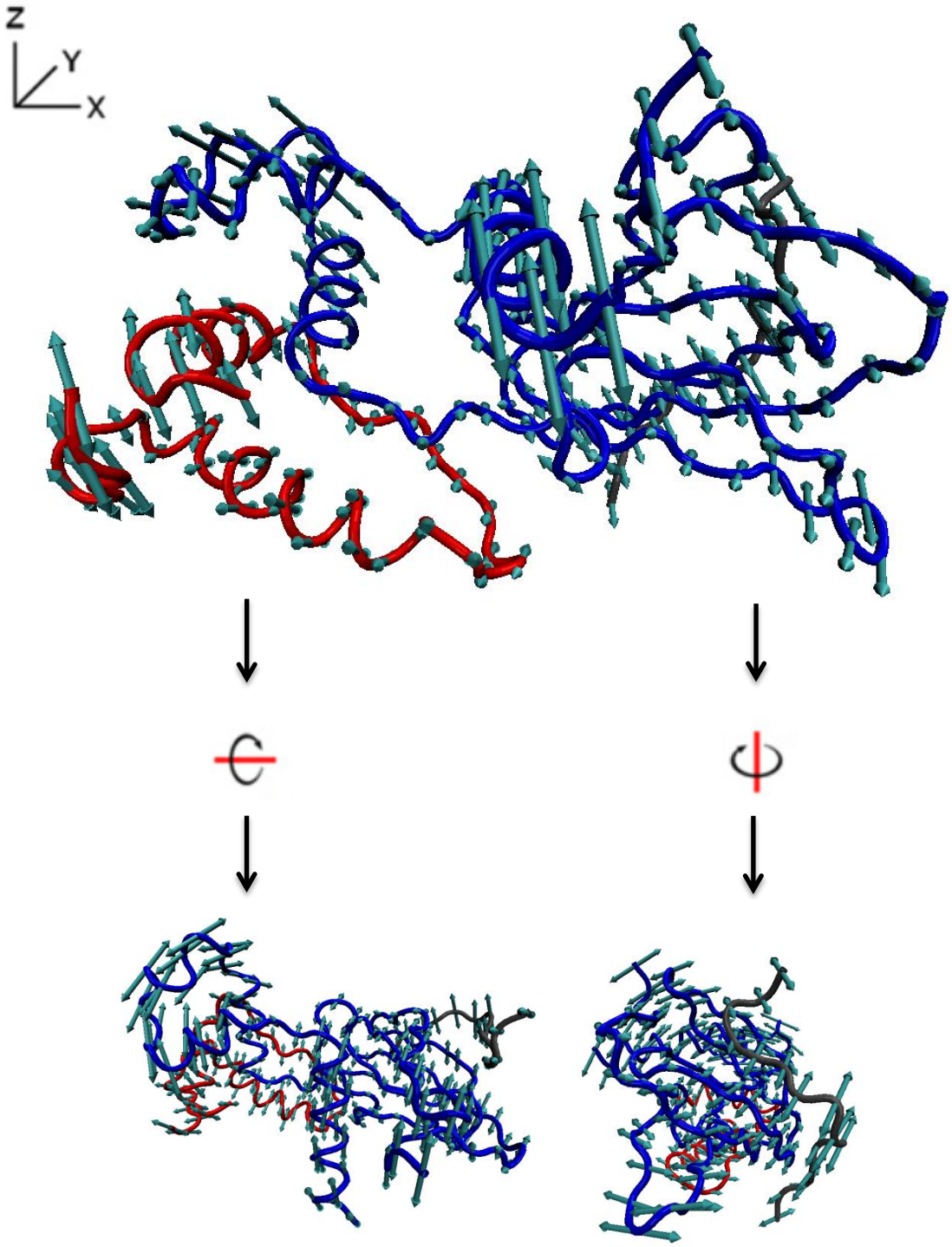

Figure 4.4 Motion of Elongin C-pVHL-HIF complex in the second slowest mode. pVHL is shown in blue, Elongin C is shown in red and HIF is shown in grey.

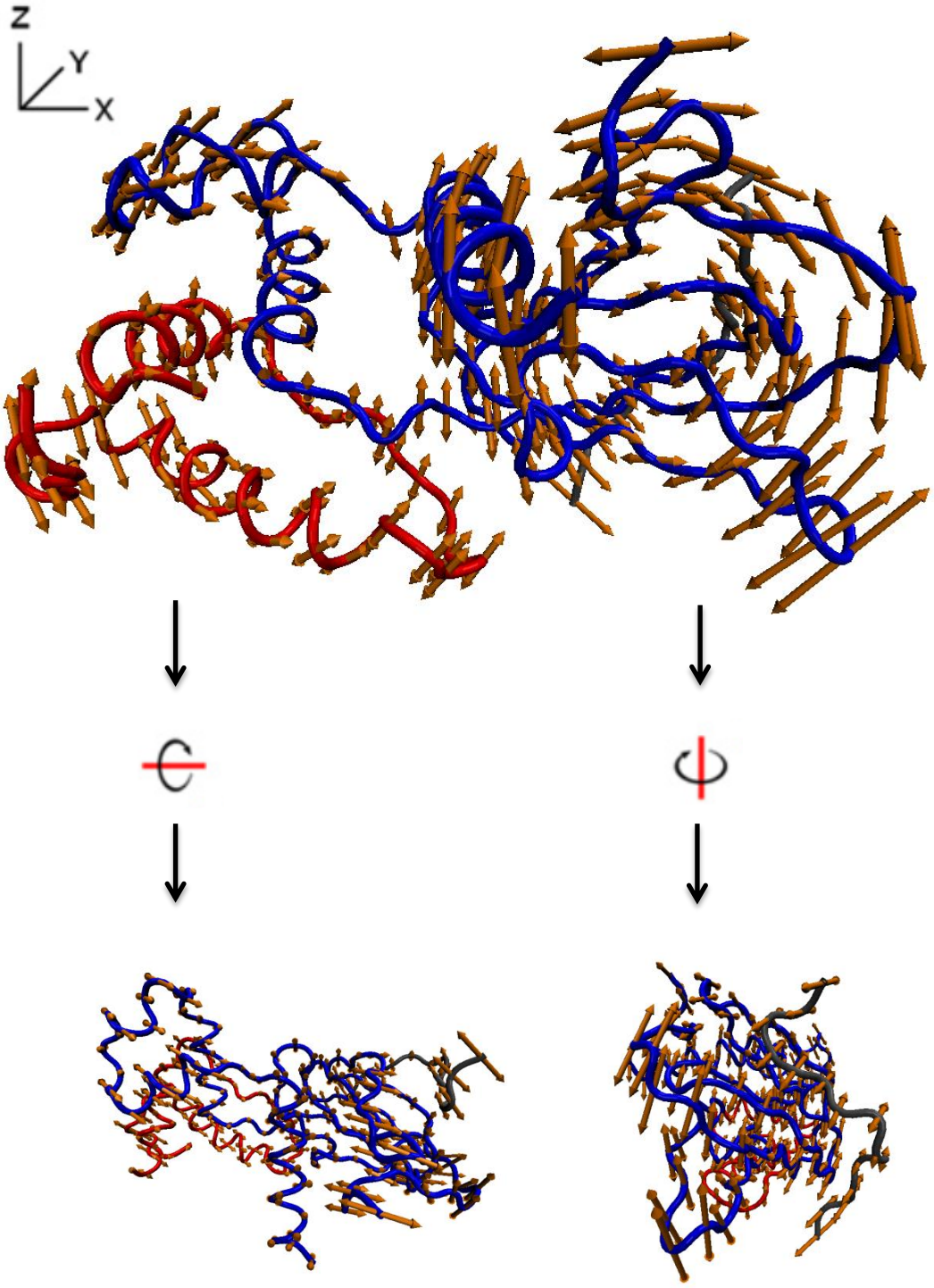

Figure 4.5 Motion of Elongin C-pVHL-HIF complex in the third slowest mode. pVHL is shown in blue, Elongin C is shown in red and HIF is shown in grey.

The mean-square fluctuations of the wild-type, the Y98N mutant, the Y98N-G123F double mutant and the Y98N-D179N double mutant pVHL complex structures were calculated for all the atoms. On Figures 4.6-8, the fluctuations of the Cα atoms in the pVHL chain in the three slowest modes are shown for clean representation. The dynamically and functionally important hinge regions correspond to the residues with the lowest fluctuation in the most cooperative functional modes of motion. The conformational changes that are functional are mainly due to the elastic deformations in the motion of these hinges that mainly determine the intrinsic dynamics and the flexibility of the Elongin C-pVHL-HIF complex. The hinge regions correspond to residues 74-76, 86-88, 95-97, 145-148 in the slowest mode (Figure 4.6); residues 78-80, 115, 150 in the second slowest mode (Figure 4.7); and residues 76, 107-109, 116-117, 136-137, 157-168 in the third slowest mode (Figure 4.8). The mode shapes of the wild-type, Y98N mutant, Y98N-G123F double mutant and Y98N-D179N double mutant structures are similar and the hinge regions in the most cooperative modes correspond to mostly the same residues. This indicates that all structures of the pVHL complex have similar fluctuation profiles with equal magnitudes of motion vectors. Therefore, a further orientational analysis was carried out to observe the changes in the directions of the motion vectors on a residue basis.

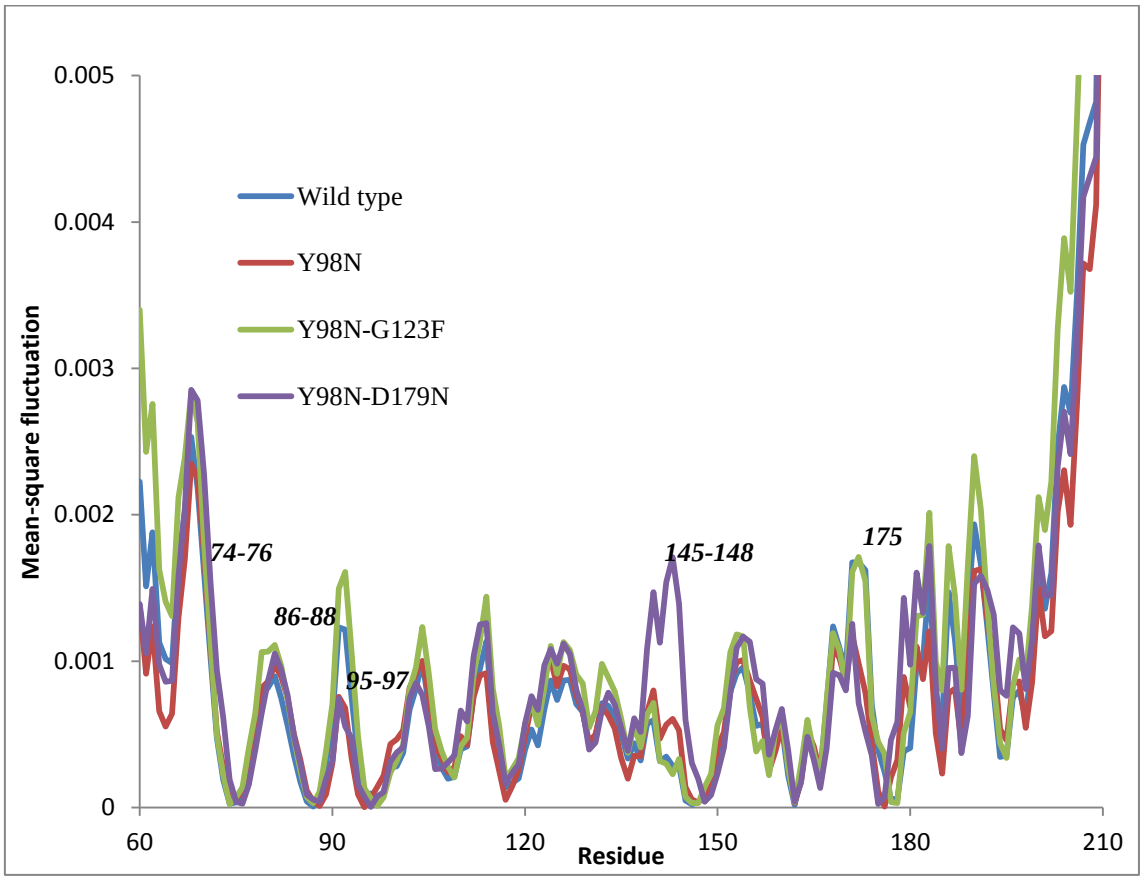

Figure 4.6 Mean square fluctuations of pVHL chain in the slowest mode (normalized).

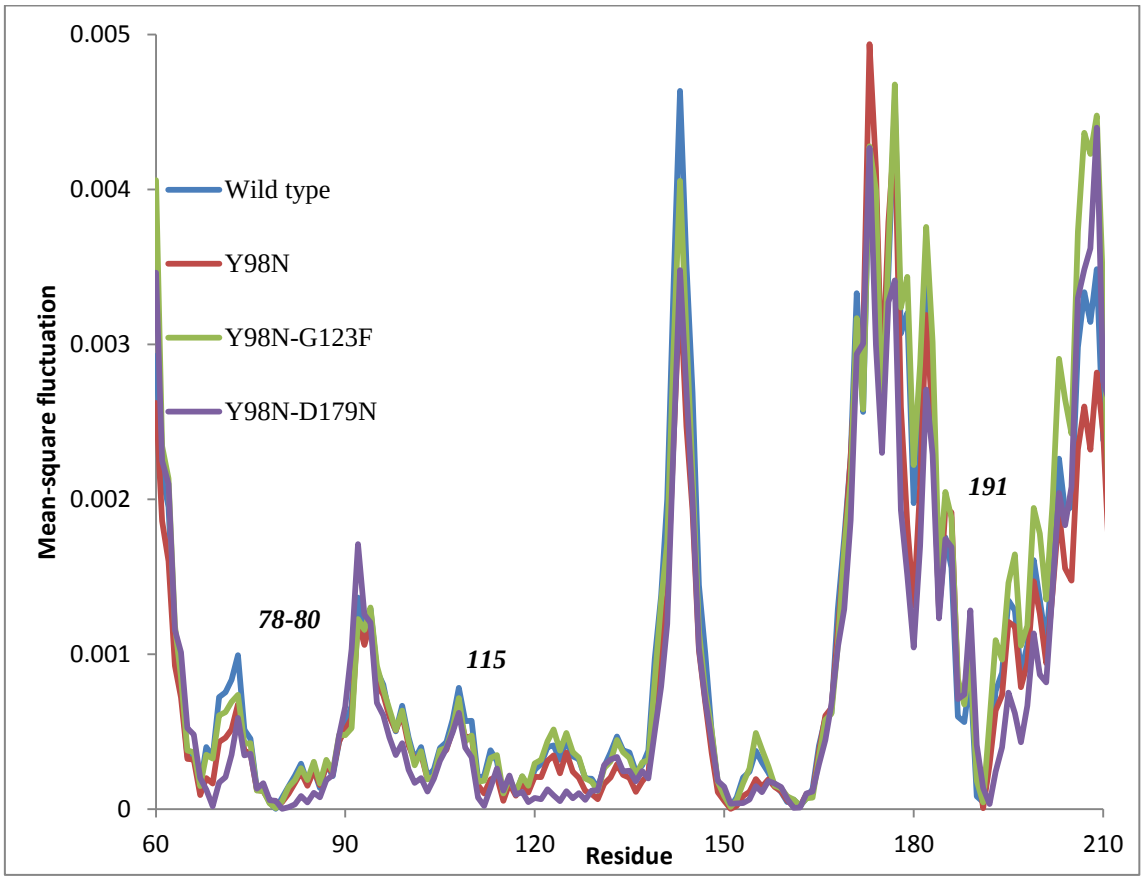

Figure 4.7 Mean square fluctuations of pVHL chain in the second slowest mode (normalized).

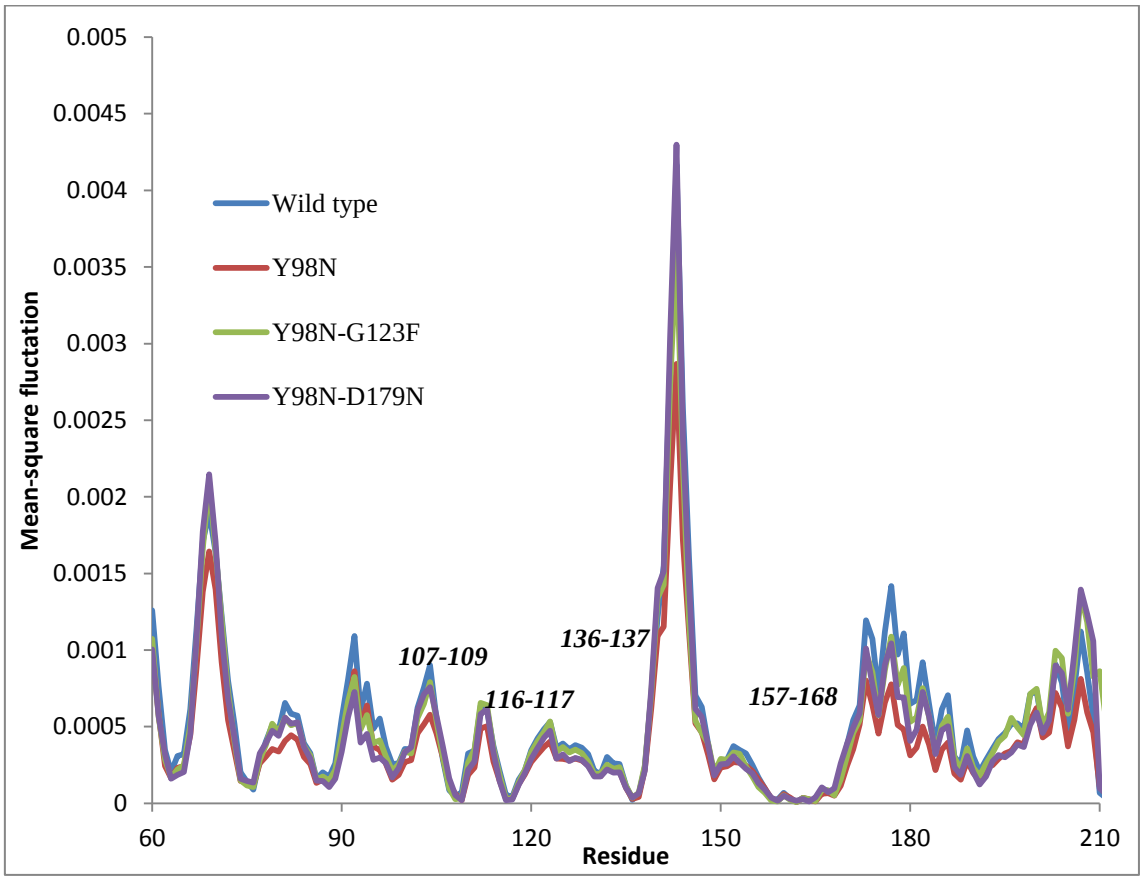

Figure 4.8 Mean square fluctuations of pVHL chain in the third slowest mode (normalized).

4.3 Orientational correlations

Even the residue mobility profiles of the pVHL variants are similar, there might be differences in the amplitude and the directionality of the fluctuation vectors. The Y98N tumor-related mutant leads disruption on functional and energetic features of the wild-type structure [4], [50]. The lower correlation between wild-type and mutant pVHL structures is not favorable and asserted as a disorder that leads to tumorigenesis. It is expected that both of the added G123F and D179N residue mutations would stabilize the tumor-related Y98N mutant separately from both thermodynamic and kinetic aspects [4]. The fluctuations in wild-type and mutant pVHL complex structures should be analyzed to evaluate the both the deformation and recovery from the tumor-related conformational state.

The inner products of eigenvectors that define the mode shapes were calculated to observe the orientational correlations between the fluctuations of the same residues in different complex structures. The orientational correlations of pVHL residues between the wild-type and mutant complex structures in the most cooperative three modes are displayed in Figures 4.9-11. The values of each residue in the charts represent the dot product value of the fluctuation vectors that define the direction of motion for that residue of the two complex structures compared. Thus, the peaks with negative correlation values in the charts indicate the residues that fluctuate more diversely thereby causing the orientational difference between the two structures compared.

The average orientational correlation values between the wild-type and the Y98N mutant is 0.96, 0.95 and 0.95, where the correlation values vary between 0.02-0.99, -0.05-0.99, and -0.99-0.99, in the slowest three modes respectively. The maximum variation in the direction of fluctuations with the tumor-related Y98N mutation is observed at residues 74, 75, 86-90, 95-99, 118, 146, 147, 174-178, 182, 185 in the slowest mode (Figure 4.9); residues 65-68, 79, 80, 82, 83, 86, 111-117, 122-125, 137, 150, 151, 157 -164, 172, 190, 191, 210 in the second slowest mode (Figure 4.10); residues 74, 75, 87, 97-99, 108, 109, 117, 131, 137, 156, 159, 161-171, 190-192, 208-210 in the third slowest mode (Figure 4.11). These residues correspond to the hinge regions with minimum fluctuation magnitudes mentioned in the previous section. Also, residues 190-210 are close to the N-terminus of the pVHL chain, where the variation in

the direction of motion near this region in the second and third slowest modes is insignificant due to high fluctuation (Figure 4.10-11). There is higher orientational correlation between the wild-type and the Y98N-G123F double mutant in all three slowest modes. That is, the average orientational correlation values between the wild-type and the Y98N-G123F double mutant is 0.98, 0.97 and 0.98, where the correlation values vary between 0.70-0.99, -0.80-0.99, and -0.50-0.99, in the slowest three modes respectively. The changes in the direction of motion of the residues that show maximum variation in the Y98N mutant are mostly recovered in the Y98N-G123F double mutant structure, except for residue 87 in the slowest mode and residues 162 and 167 in the third slowest mode. The increment in the orientational correlation values are roughly by 0.3 in the Y98N-G123F double mutant structure. Since these residues correspond to the functionally important hinge regions (Figure 4.12), the increment in the average orientational correlation values with the G123F mutation implies significant regain of the wild type dynamical state by the G123F mutation. However, this cannot be observed in the Y98N-D179N double mutant, where the average orientational correlation values for each residue decrease remarkably compared to the Y98N mutant in the most cooperative modes. The average orientational correlation values between the wild-type and the Y98N-D179N double mutant is 0.91, 0.90 and 0.96 in the slowest three modes respectively.

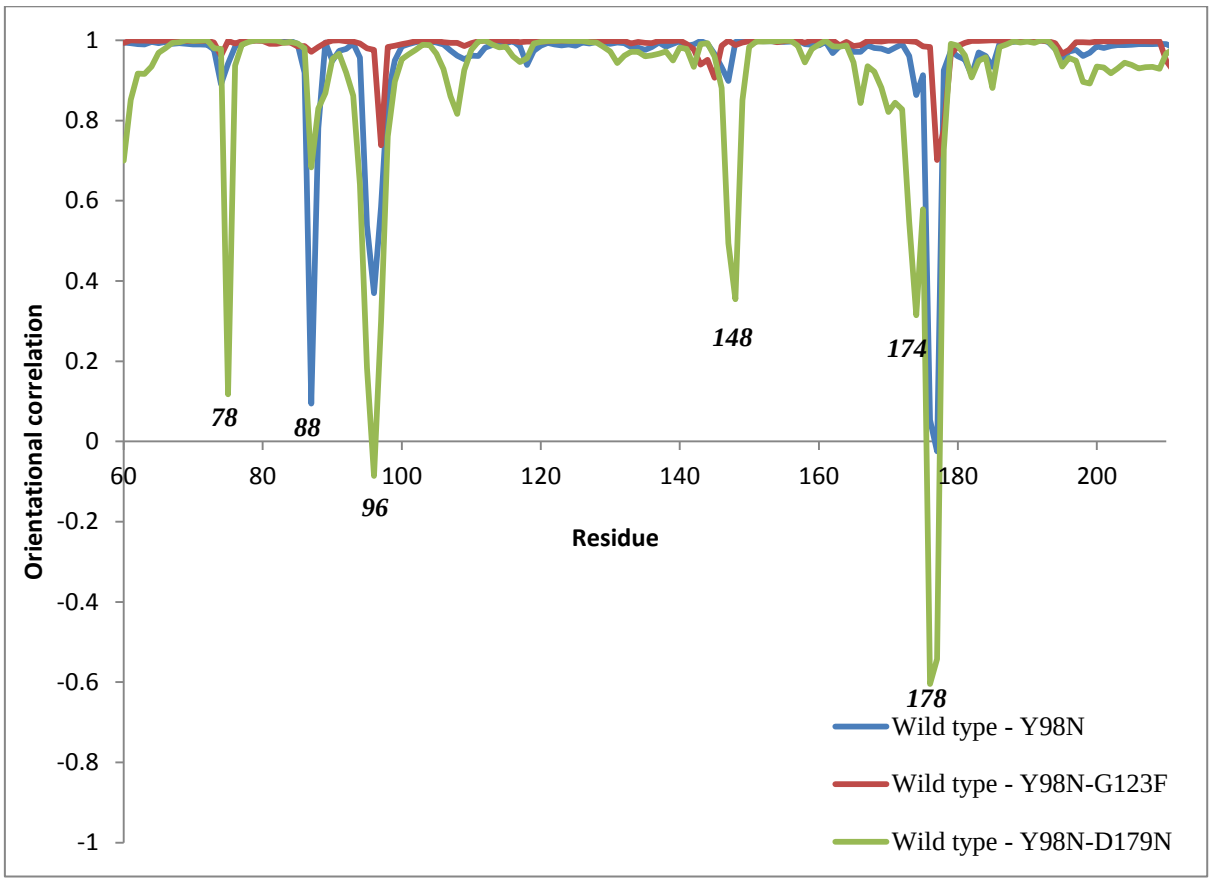

Figure 4.9 Orientational correlations in the slowest mode.

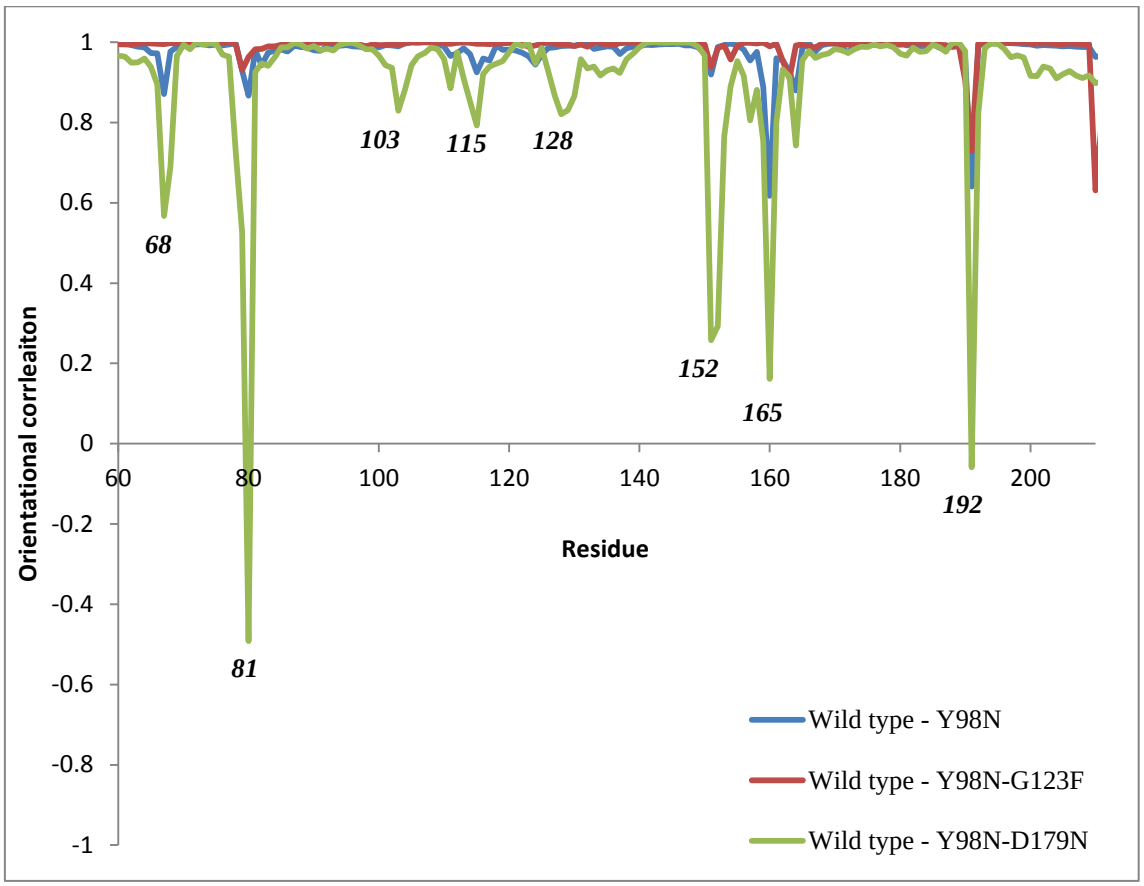

Figure 4.10 Orientational correlations in the second slowest mode.

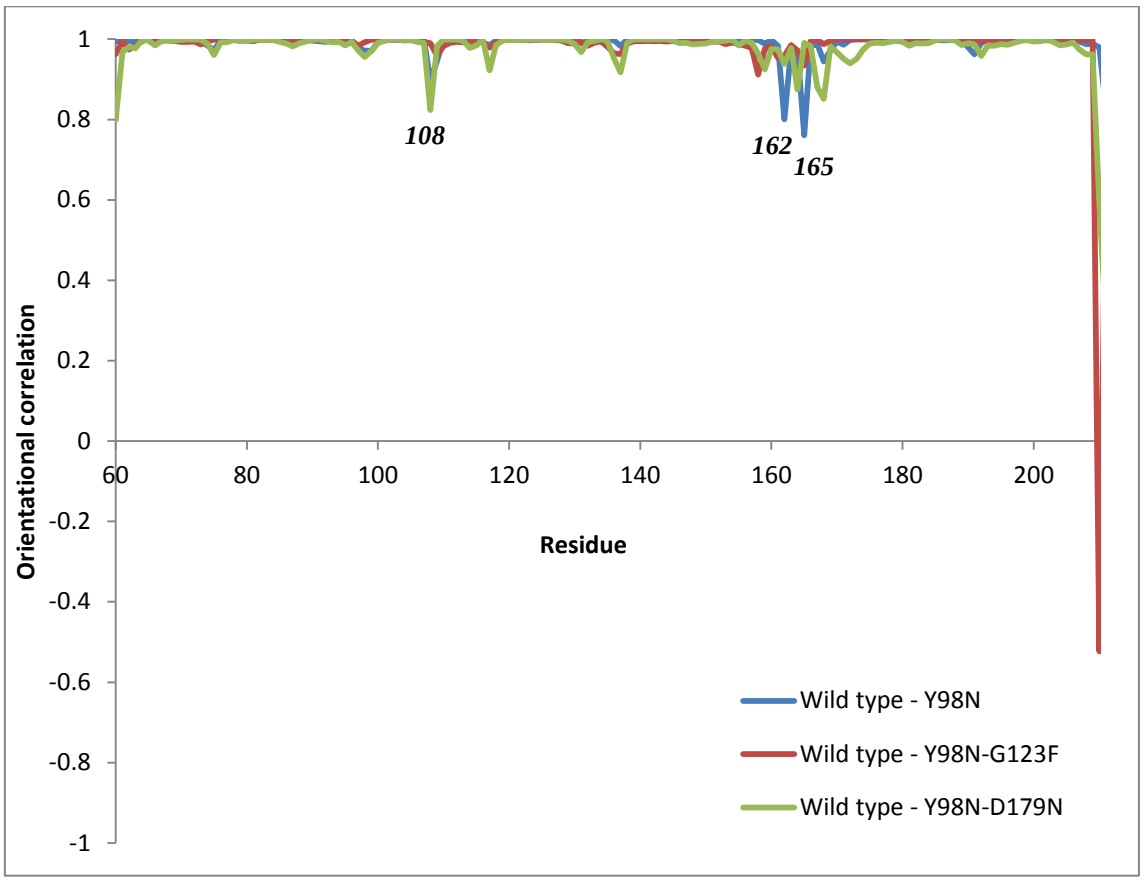

Figure 4.11 Orientational correlations in the third slowest mode.

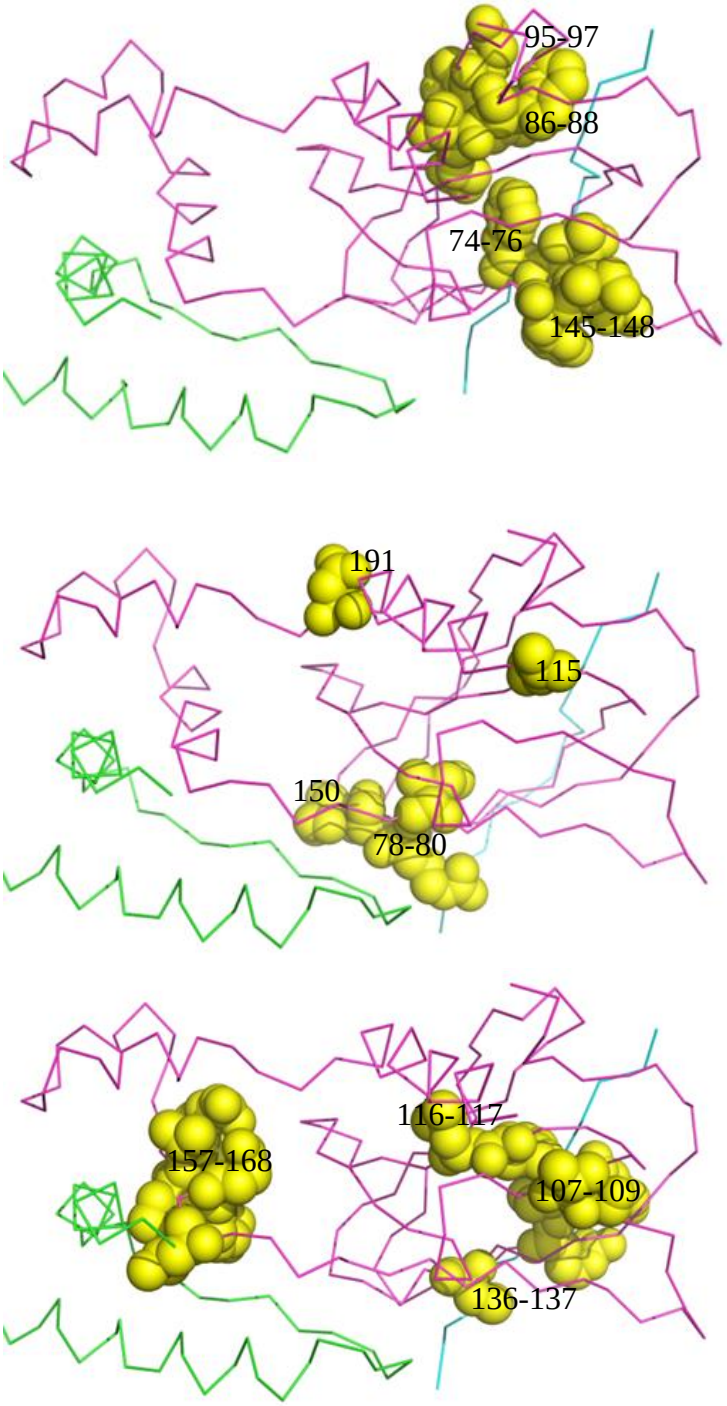

Figure 4.12 Hinge residues that lead to orientational difference between the wild-type and Y98N-G123F double mutant structures. The slowest mode (A), the second slowest mode (B) and the third slowest mode (C) are shown.

4.4 Cross-correlations between fluctuations

The correlations between the fluctuations of the residues- are displayed for the average of the slowest ten modes in Figures 4.13-16 for the wild-type, the Y98N mutant, the Y98N-G123F double mutant and the Y98N-D179N double mutant pVHL complex structures, respectively. The cross-correlation analysis was carried out with all atoms of each structure, yet the heatmaps are shown only for the carbon alpha atoms for a clearer view. The regions which correspond to the minima in the mean-square fluctuations are observed to be highly positively correlated with each other. H1 helix and L2, L6, L8 loops of the pVHL chain that are important for Elongin C-pVHL binding have significant positive correlations between each other in the wild-type and all mutant structures. However, the positive inner correlations of the pVHL chain in the Y98N mutant are considerably higher than those in the wild type, and double mutant structures. Also, the positive correlations between pVHL and Elongin C chains are notably higher in the Y98N mutant structure compared to the others. These strong positive correlations in the tumor-related Y98N mutant structure suggest that there is deformation of the dynamic behavior of the Elongin C-pVHL-HIF complex due to the tumor-related mutation.

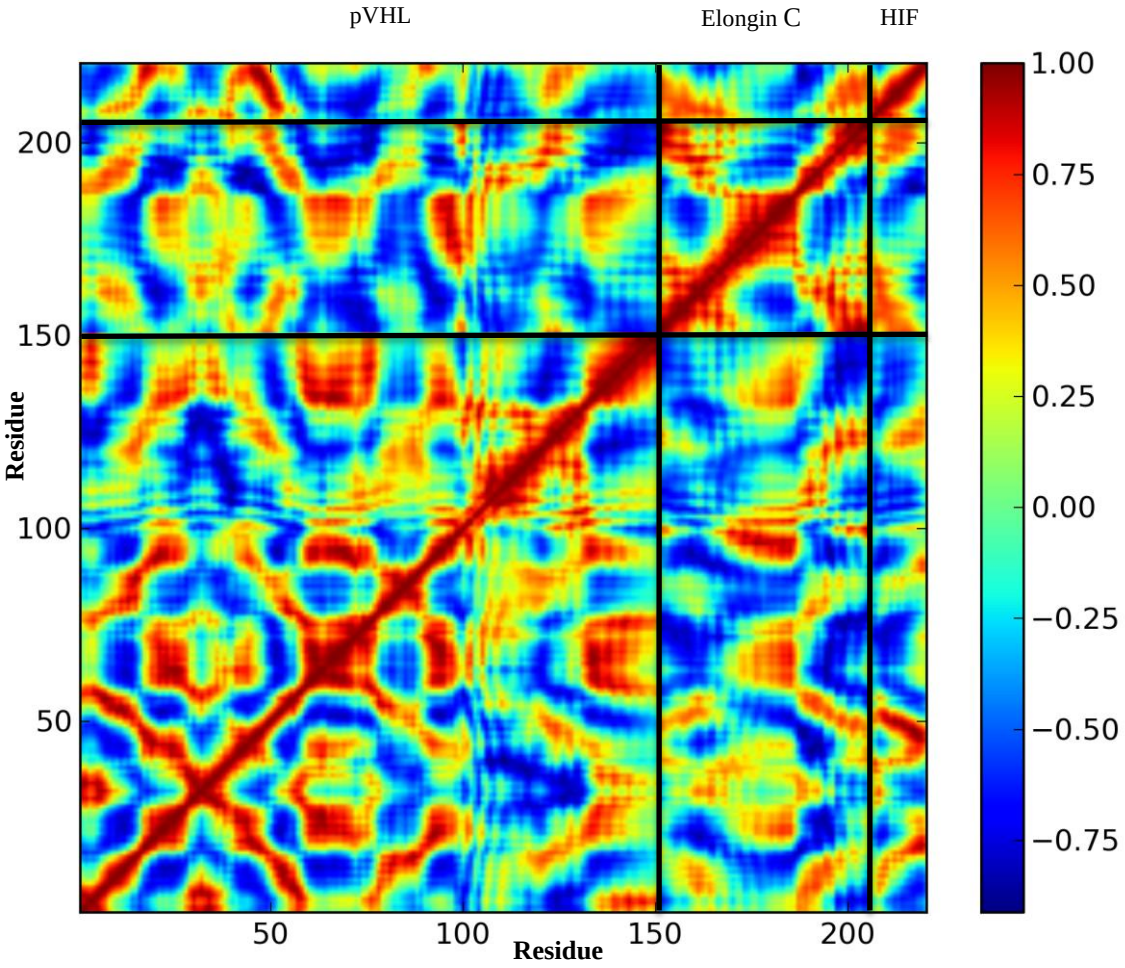

Figure 4.13 Cross-correlations between the fluctuations of residues in the wild-type Elongin C-pVHL-HIF structure (only carbon alpha atoms are displayed).

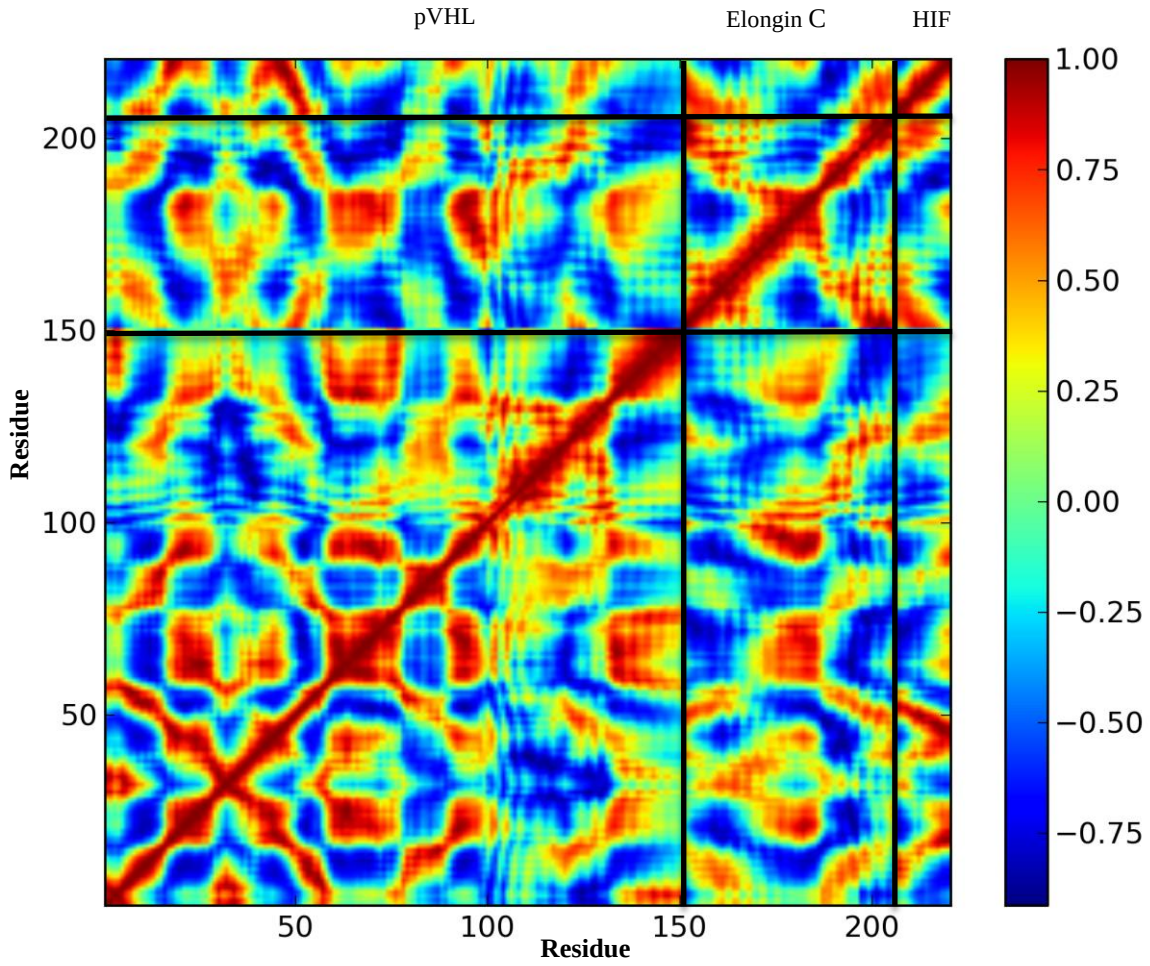

Figure 4.14 Cross-correlations between the fluctuations of residues in the Y98N mutant Elongin C-pVHL-HIF structure (only carbon alpha atoms are displayed).

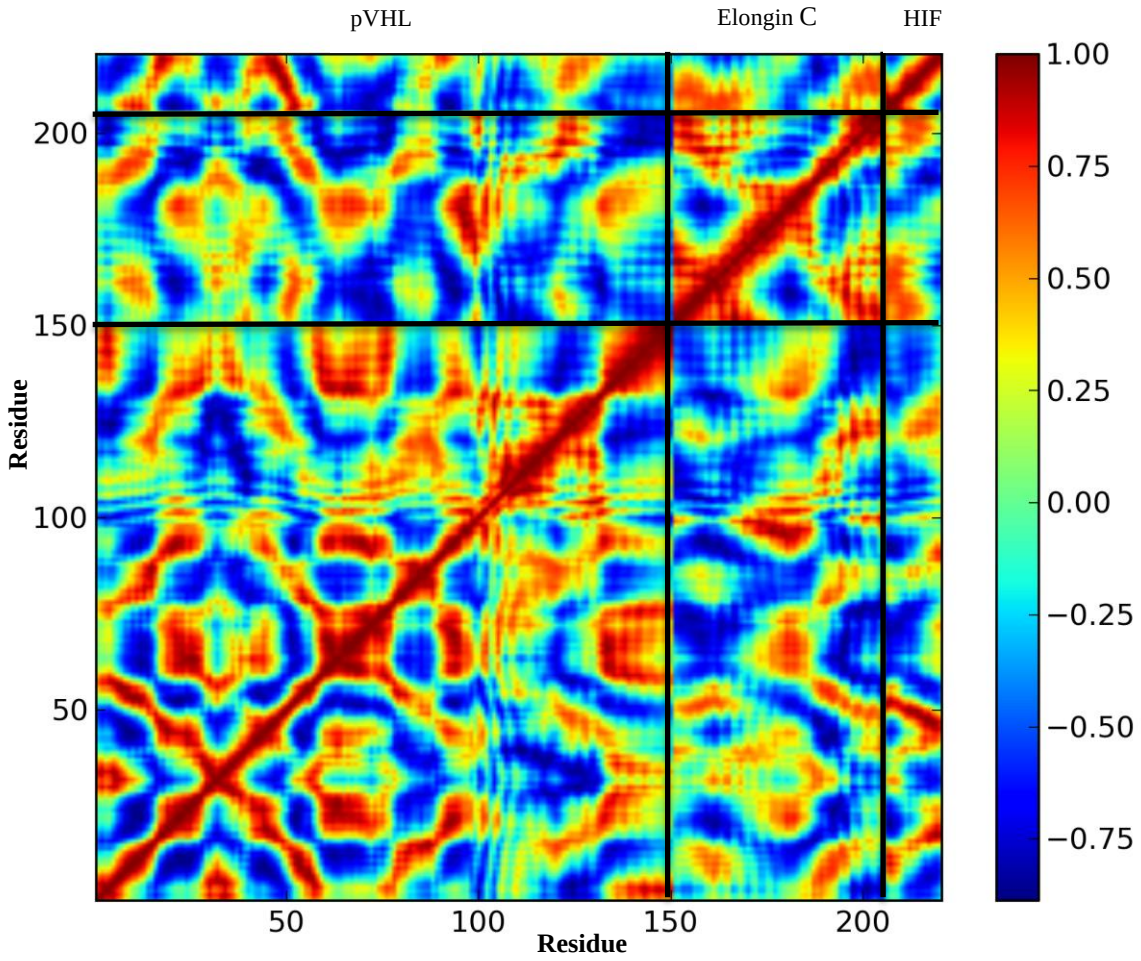

Figure 4.15 Cross-correlations between the fluctuations of residues in the Y98N-G123F mutant Elongin C-pVHL-HIF structure (only carbon alpha atoms are displayed).

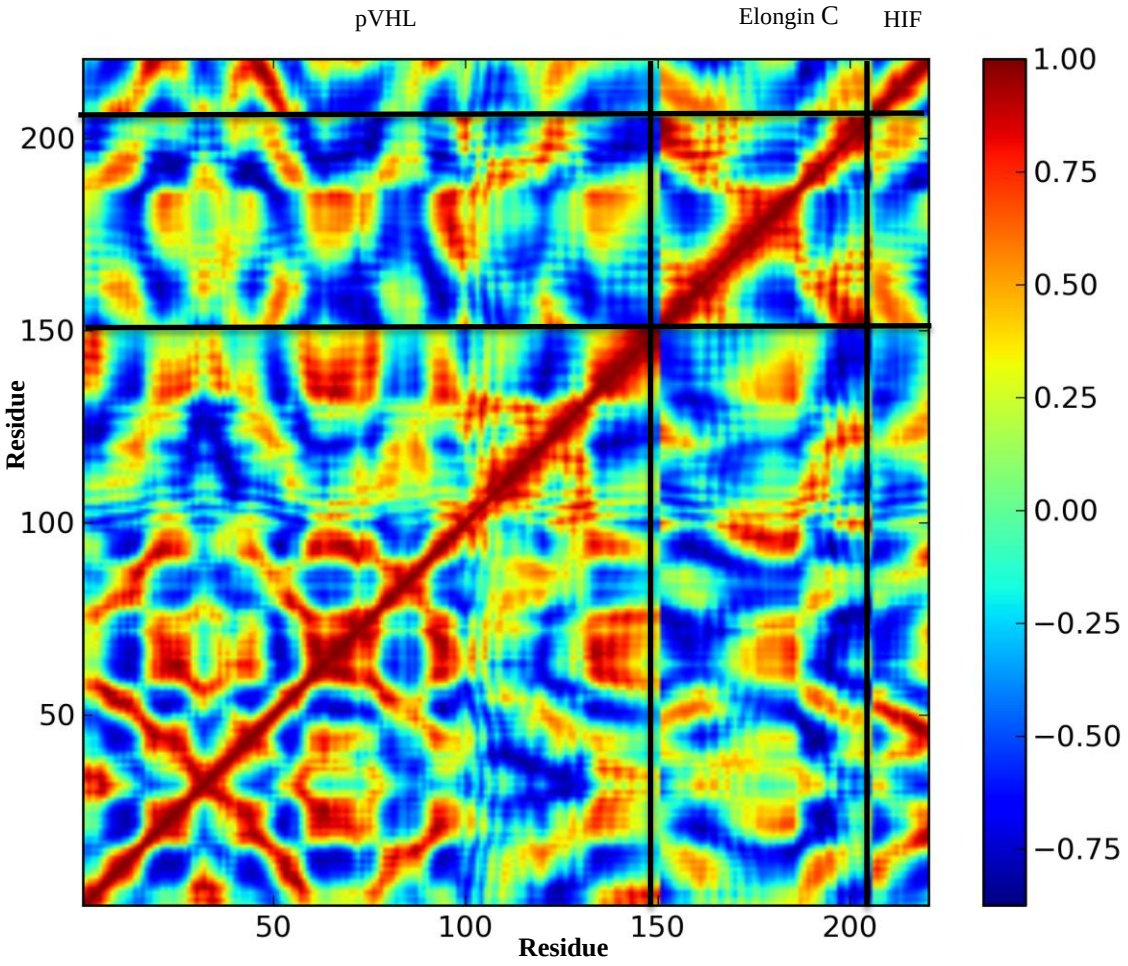

Figure 4.16 Cross-correlations between the fluctuations of residues in the Y98N-D179N mutant Elongin C-pVHL-HIF structure (only carbon alpha atoms are displayed).

The cross-correlations between the residue fluctuations suggest a comparison between the dynamic behavior of the different chains of the protein complex. Previous studies suggest that interdomain relation within the Elongin C-pVHL-HIF complex is important for dynamical stability and for functioning properly as a tumor regulator [21]. The positive correlations between residue fluctuations are more pronounced and significant within the pVHL chain in the Y98N mutant compared to those in the wild-type, the Y98N-G123F and the Y98N-D179N double mutant structures. Between pVHL and Elongin C chains, there is a higher number of positive correlations in the Y98N mutant, compared to the wild-type, the Y98N-G123F and the Y98N-D179N double mutant structures. Between the pVHL and the HIF chains, on the other hand, there is a higher number of positive correlations in the Y98N mutant compared to the wild-type structure, yet the number of positive correlations do not decrease in the Y98N-G123F and the Y98N-D179N double mutant structures. The number of positive correlations above 0.8 is shown on Table 4.4. The total positive correlations within the Elongin C-pVHL-HIF complex are 40% higher in number in the tumor-related Y98N mutant compared to the other structures. The number of positive correlations within the pVHL chain increase roughly 20% in the Y98N mutant while the wild type and double mutant structures has very close values. The number of positive correlations between Elongin C and pVHL chains is also highest in the Y98N mutant structure compared to the other structures.

Table 4.4 The number of positive correlations above 0.8.

	Wild-type	Y98N	Y98N-G123F	Y98N-D179N
In Elongin C-pVHL-HIF complex	2640	3582	2760	2688
Between pVHL and Elongin C chains	59	264	67	55
Between pVHL and HIF chains	40	55	53	59
In pVHL chain	1826	2276	1894	1866

The regions that are significant in binding between pVHL and Elongin C chains are evaluated with the positive correlations between the residue fluctuations (Figures 4.17-20). L8 loop of the pVHL chain shows similar correlation with Elongin C in the wild-type (Figure 4.17), the Y98N-G123F double mutant (Figure 4.19) and the Y98N-D179N double mutant (Figure 4.20) structures. In the tumor-related Y98N mutant structure (Figure 4.18), L2, L4, L8 and L11 loops of the pVHL chain display higher correlation with Elongin C. Higher positive correlations in the Elongin C-pVHL interface indicate higher binding affinity between these chains in the tumor-related mutant. This binding affinity is altered by either G123F or D179N mutations and the wild-type dynamic behavior is regained.

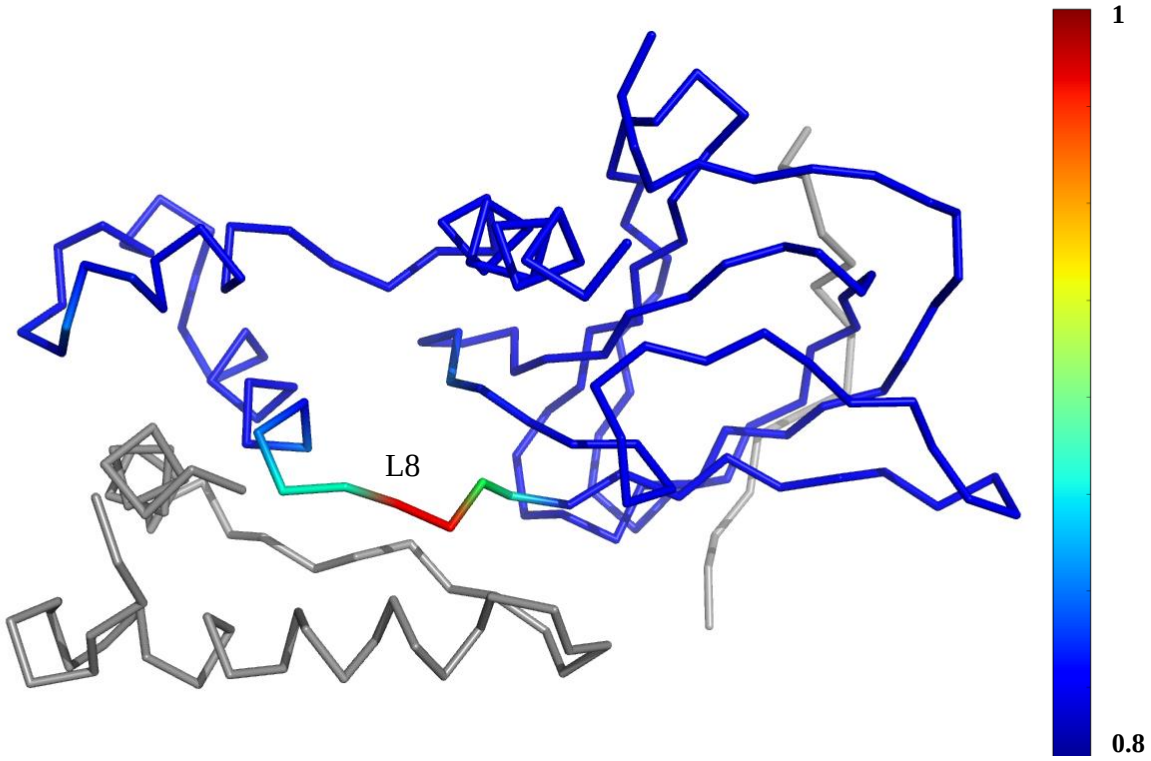

Figure 4.17 pVHL regions significant for binding to Elongin C in the wild-type.

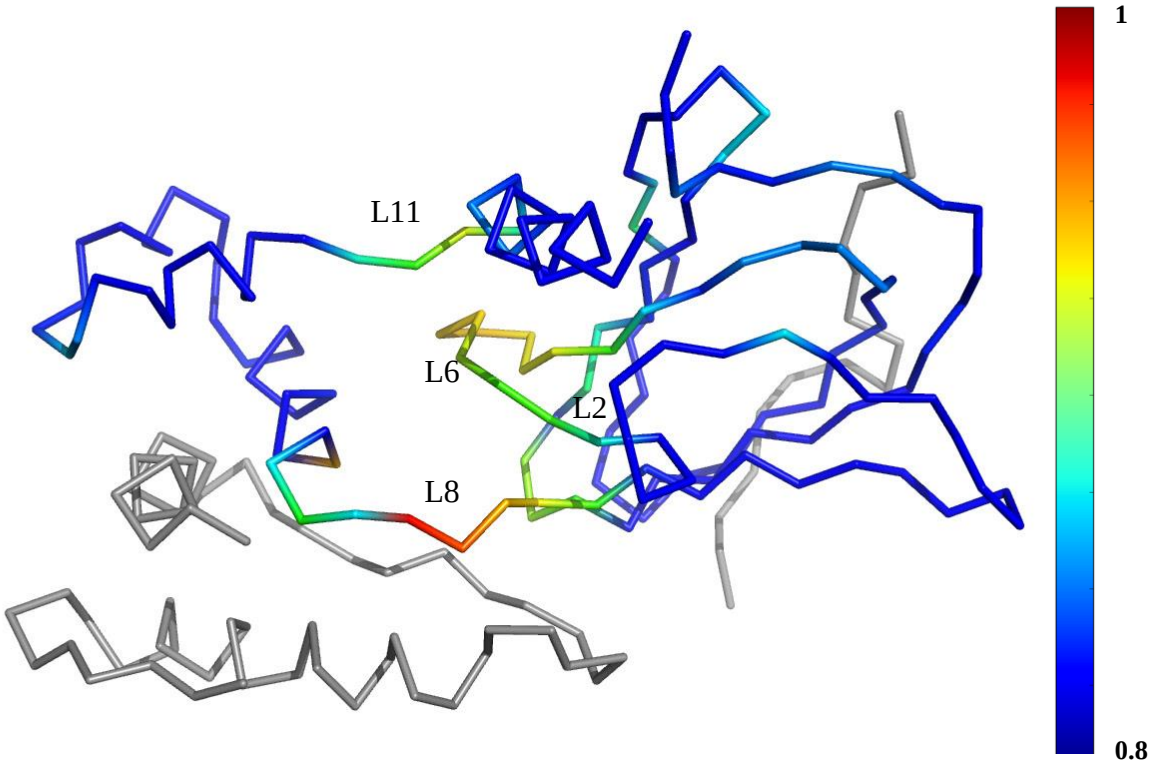

Figure 4.18 pVHL regions significant for binding to Elongin C in the Y98N mutant.

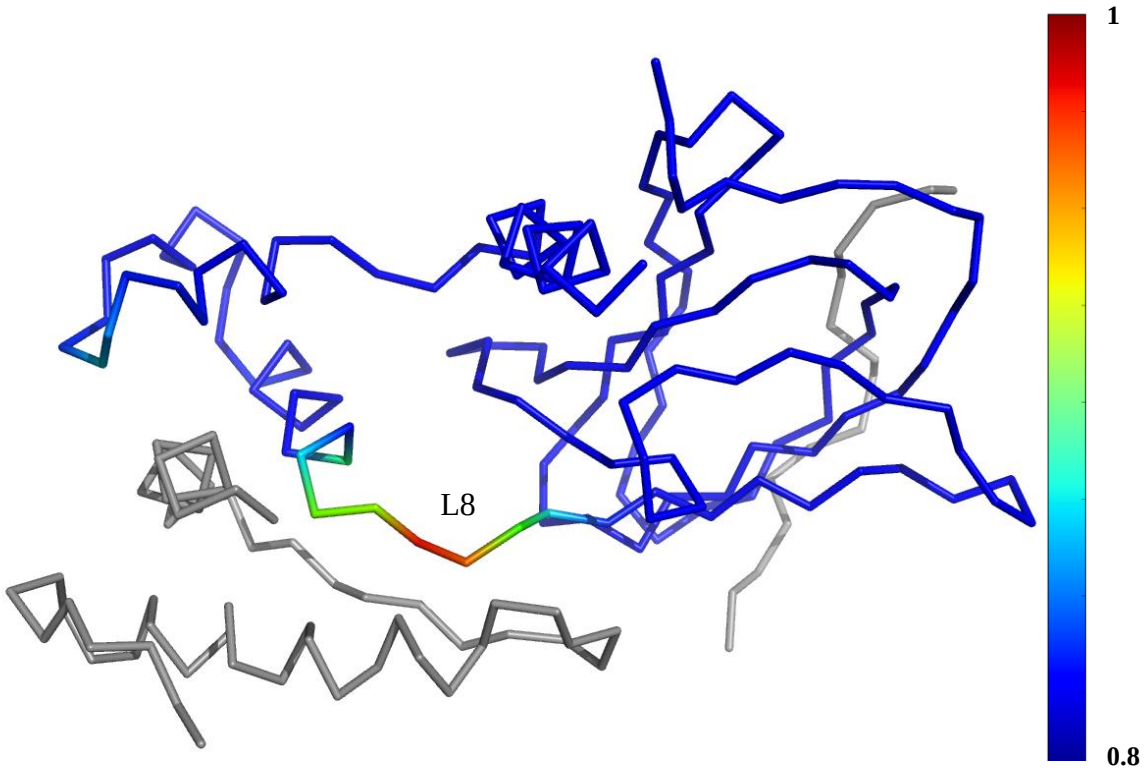

Figure 4.19 pVHL regions significant for binding to Elongin C in the Y98N-G123F mutant.

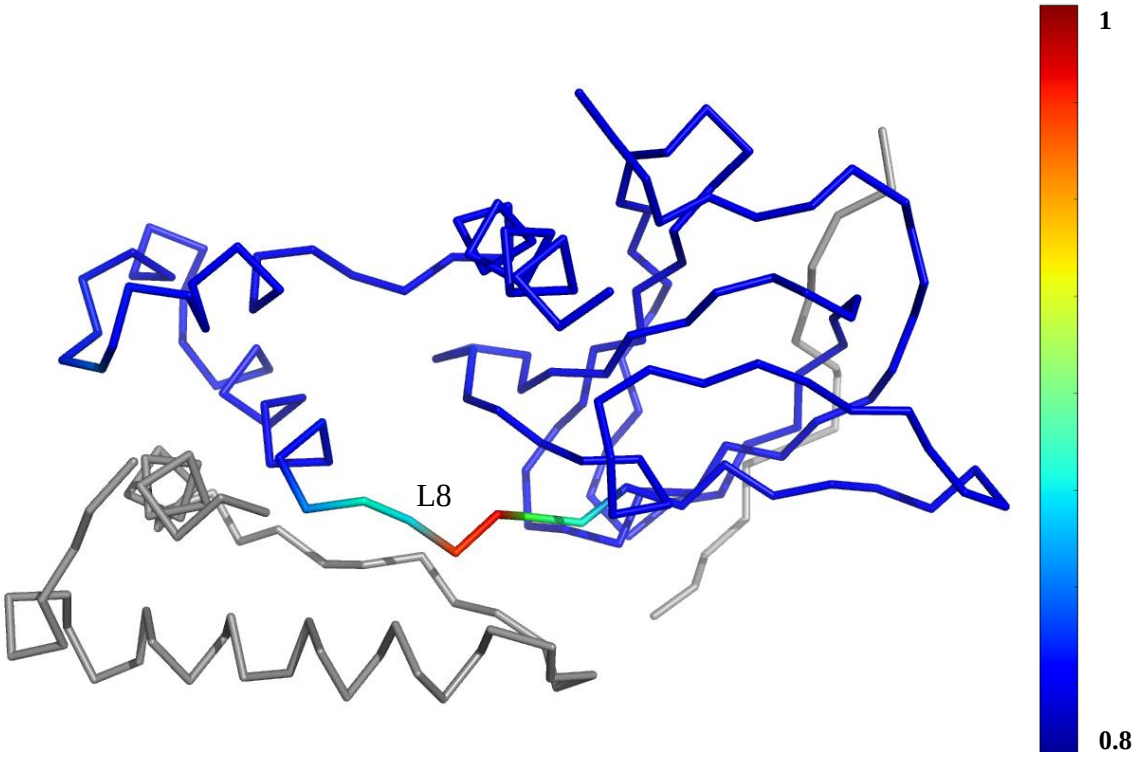

Figure 4.20 pVHL regions significant for binding to Elongin C in the Y98N mutant.

CHAPTER 5 CONCLUSIONS AND RECOMMENDATIONS

The biological function of proteins is mainly maintained and inherited by the preservation of dynamic properties. Therefore, structural dynamics studies in proteins lead to comprehension of their preserved evolutionary and functional properties. The global motions of the proteins can be defined by the most cooperative normal modes of elastic network models. These modes demonstrate the highest relevance to the flexibility patterns, and they are essentially determined by the proteins' amino acid composition. Thus, they are generally evolutionarily conserved and functionally relevant. Likewise, the hinge regions observed in these conserved modes of motion are shown to play crucial roles in the conformations induced by perturbations.

In this thesis, the ANM was used as the computational tool to analyze the structural dynamics of the pVHL system. The dynamics of the three most cooperative modes of pVHL complex was analyzed with the wild-type, the in silico designed tumor-related Y98N mutant, the in silico designed Y98N-G123F double mutant and the in silico designed Y98N-D179N double mutant structures. The slowest modes contributed to nearly 50% of the overall motion, and the investigation of these modes presented adequate information about the collective dynamics of the protein. The results indicated that the wild-type and the designed double mutant structures exhibit similar dynamic behavior. That is, by inserting secondary mutations, the deformation in the dynamic behavior caused by the tumor-related Y98N substitution could be recovered. The information gathered from these analyses on the pVHL protein system would help in the drug design studies for the VHL disease. Drugs which affect the pVHL system that lead the same recovery like the in silico designed mutants could improve cancer treatments and enlighten the underlying factor for the tumor-related diseases.

For future study, it is recommended that designing other double mutants for the pVHL system could help investigating the mechanism of recovery from the tumor-related state. Longer MD simulations with different force-fields and trials of cluster analyses with different algorithms are also recommended.

REFERENCES

[1] P. E. Clark, “The role of VHL in clear-cell renal cell carcinoma and its relation to targeted therapy,” *Kidney Int.*, vol. 76, no. 9, pp. 939–945, Nov. 2009.

[2] R. R. Lonser, G. M. Glenn, M. Walther, E. Y. Chew, S. K. Libutti, W. M. Linehan, and E. H. Oldfield, “Von Hippel-Lindau disease,” *Lancet*, vol. 361, pp. 2059–2067, 2003.

[3] C. E. Stebbins, W. G. Kaelin, and N. P. Pavletich, “Structure of the VHL-ElonginC-ElonginB complex: implications for VHL tumor suppressor function.,” *Science*, vol. 284, no. April 1999, pp. 455–461, 1999.

[4] J. Liu and R. Nussinov, “Allosteric effects in the marginally stable von Hippel-Lindau tumor suppressor protein and allostery-based rescue mutant design.,” *Proc. Natl. Acad. Sci. U. S. A.*, vol. 105, no. 3, pp. 901–906, 2008.

[5] a R. Atilgan, S. R. Durell, R. L. Jernigan, M. C. Demirel, O. Keskin, and I. Bahar, “Anisotropy of fluctuation dynamics of proteins with an elastic network model.,” *Biophys. J.*, vol. 80, no. 1, pp. 505–15, Jan. 2001.

[6] E. T. Collins, “Intra-ocular growths (two cases, brother and sister, with peculiar vascular new growth, probably primarily retinal, affecting both eyes),” *Trans. Ophthal. Soc. UK*, vol. 14, pp. 141–149, 1894.

[7] K. L. Melmon and S. W. Rosen, “Lindau’s disease. Review of the literature and study of a large kindred,” *Am. J. Med.*, vol. 36, pp. 595–617, 1964.

[8] D. DR, H. JS, C. CYT, Y. Weng, J. Sukegawa, S. Lee, G. JR, L. WM, and K. RD, “Characterization of the VHL tumor suppressor gene product: Localization complex formation and the effect of naturally inactivating mutations,” *Proc Nat Acad Sci USA*, vol. 92, pp. 6363–6459, 1995.

[9] A. Kibel, O. Iliopoulos, D. JA, and K. W. G. JR, “Binding of the von Hippel-Lindau tumor suppressor protein to Elongin B and C,” *Science (80-.).*, vol. 269, pp. 1444–1446, 1995.

[10] K. M. Lonergan, “Regulation of hypoxia-inducible mRNAs by the von Hippel-Lindau tumor suppressor protein requires binding to complexes containing elongins B/C and Cul2,” *Mol. Cell. Biol.*, vol. 18, pp. 732–741, 1998.

[11] O. Iliopoulos, A. Kibel, S. Gray, and K. W. G. JR, “Tumor suppression by the human von Hippel-Lindau gene product,” *Nat. Med*, vol. 1, pp. 822–826, 1995.

[12] O. Iliopoulos, A. P. Levy, C. Jiang, W. G. Kaelin Jr, and M. A. Goldberg, “Negative regulation of hypoxia-inducible genes by the von Hippel-Lindau protein,” *Proc. Natl Acad. Sci. USA*, vol. 93, pp. 10595–10599, 1996.

[13] S. BR, R. GA, O. LJ, L. AH, F. GE, L. JM, J. Haines, Y. JWM, D. Collins, D. Majoor-Krakauer, T. Bonner, C. Mathew, A. Rubenstein, J. Halperin, A. Mcconkie-Rosell, G. JS, T. JA, P. BA, L. Eierman, B. MI, R. Schimke, B. Oostra, N. Aronin, S. DI, H. Drabkin, W. MH, H. WJ, M. RL, C. PM, H. YE, and G. JF, "Von Hippel-Lindau disease maps to the region of chromosome 3 associated with renal cell carcinoma," *Nature*, vol. 332, pp. 268–269, 1988.

[14] C. Stolle, G. Glenn, B. Zbar, J. S. Humphrey, P. Choyke, M. Walther, S. Pack, K. Hurley, C. Andrey, R. Klausner, and W. M. Linehan, "Improved detection of germline mutations in the von Hippel-Lindau disease tumor suppressor gene," *Hum. Mutat.*, vol. 12, no. 6, pp. 417–423, 1998.

[15] J. R. Gnarra, K. Tory, Y. Weng, L. Schmidt, M. H. Wei, H. Li, F. Latif, S. Liu, F. Chen, F.-M. M. Duh, I. Lubensky, D. R. Duan, C. Florence, R. Pozzatti, M. M. Walther, N. H. Bander, H. B. Grossman, H. Brauch, S. Pomer, J. D. Brooks, W. B. Isaacs, M. I. Lerman, B. Zbar, and W. M. Linehan, "Mutations of the VHL tumour suppressor gene in renal carcinoma," *Nat Genet*, vol. 7, no. 1, pp. 85–90, May 1994.

[16] A. Pause, S. Lee, K. M. Lonergan, and R. D. Klausner, "The von Hippel-Lindau tumor suppressor gene is required for cell cycle exit upon serum withdrawal," *Proc. Natl Acad. Sci. USA*, vol. 95, pp. 993–998, 1998.

[17] a R. Schoenfeld, E. J. Davidowitz, and R. D. Burk, "Elongin BC complex prevents degradation of von Hippel-Lindau tumor suppressor gene products.," *Proc. Natl. Acad. Sci. U. S. A.*, vol. 97, pp. 8507–8512, 2000.

[18] M. E. Cockman, N. Masson, D. R. Mole, P. Jaakkola, G. W. Chang, S. C. Clifford, E. R. Maher, C. W. Pugh, P. J. Ratcliffe, and P. H. Maxwell, "Hypoxia inducible factor-α binding and ubiquitylation by the von Hippel-Lindau tumor suppressor protein," *J. Biol. Chem.*, vol. 275, pp. 25733–25741, 2000.

[19] M. Ohh, "Ubiquitination of hypoxia-inducible factor requires direct binding to the [beta]-domain of the von Hippel-Lindau protein," *Nat. Cell Biol.*, vol. 2, pp. 423–427, 2000.

[20] L. Gossage, "Clinical and pathological impact of VHL, PBRM1, BAP1, SETD2, KDM6A, and JARID1c in clear cell renal cell carcinoma," *Genes Chromosom. Cancer*, vol. 53, pp. 38–51, 2014.

[21] L. Gossage, T. Eisen, and E. R. Maher, "VHL, the story of a tumour suppressor gene," *Nat. Publ. Gr.*, vol. 15, no. 1, pp. 55–64, 2015.

[22] K. Knauth, C. Bex, P. Jemth, and a Buchberger, "Renal cell carcinoma risk in type 2 von Hippel-Lindau disease correlates with defects in pVHL stability and HIF-1alpha interactions.," *Oncogene*, vol. 25, pp. 370–377, 2006.

[23] G. Limaverde-Sousa, E. de Andrade Barreto, C. G. Ferreira, and J. Cláudio Casali-da-Rocha, “Simulation of the mutation F76del on the von Hippel-Lindau tumor suppressor protein: Mechanism of the disease and implications for drug development,” *Proteins Struct. Funct. Bioinforma.*, vol. 81, no. September, pp. 349–363, 2013.

[24] G. Minervini, A. Masiero, S. Moro, and S. C. E. Tosatto, “In silico investigation of PHD-3 specific HIF1-?? proline 567 hydroxylation: A new player in the VHL/HIF-1?? interaction pathway?,” *FEBS Lett.*, vol. 587, no. 18, pp. 2996–3001, 2013.

[25] L. Gossage, D. E. V Pires, Á. Olivera-Nappa, J. Asenjo, M. Bycroft, T. L. Blundell, T. Eisen, Á. O. Nappa, and J. Asenjo, “An integrated computational approach can classify VHL missense mutations according to risk of clear cell renal carcinoma,” *Hum. Mol. Genet.*, vol. 23, no. 22, pp. 5976–5988, Nov. 2014.

[26] I. Bahar, T. R. Lezon, L.-W. Yang, and E. Eyal, “Global dynamics of proteins: bridging between structure and function.,” *Annu. Rev. Biophys.*, vol. 39, pp. 23–42, 2010.

[27] S. Nicolay and Y. H. Sanejouand, “Functional modes of proteins are among the most robust,” *Phys. Rev. Lett.*, vol. 96, no. February, pp. 1–4, 2006.

[28] A. L. Tournier and J. C. Smith, “Principal components of the protein dynamical transition.,” *Phys. Rev. Lett.*, vol. 91, no. 1, p. 208106, 2003.

[29] L. Skjaerven, S. M. Hollup, and N. Reuter, “Normal mode analysis for proteins,” *J. Mol. Struct. THEOCHEM*, vol. 898, no. 1–3, pp. 42–48, 2009.

[30] J. Ma, “Usefulness and limitations of normal mode analysis in modeling dynamics of biomolecular complexes,” *Structure*, vol. 13, pp. 373–380, 2005.

[31] C. Chennubhotla, a J. Rader, L.-W. Yang, and I. Bahar, “Elastic network models for understanding biomolecular machinery: from enzymes to supramolecular assemblies.,” *Phys. Biol.*, vol. 2, pp. S173–S180, 2005.

[32] P. Gniewek, A. Kolinski, R. L. Jernigan, and A. Kloczkowski, “Elastic network normal modes provide a basis for protein structure refinement,” *J. Chem. Phys.*, vol. 136, pp. 1–10, 2012.

[33] M. Tirion, “Large Amplitude Elastic Motions in Proteins from a Single-Parameter, Atomic Analysis.,” *Phys. Rev. Lett.*, vol. 77, no. 9, pp. 1905–1908, Aug. 1996.

[34] T. Haliloglu, I. Bahar, and B. Erman, “Gaussian Dynamics of Folded Proteins,” *Phys. Rev. Lett.*, vol. 79, no. 16, pp. 3090–3093, Oct. 1997.

[35] I. Bahar, a R. Atilgan, and B. Erman, “Direct evaluation of thermal fluctuations in proteins using a single-parameter harmonic potential.,” *Fold. Des.*, vol. 2, pp. 173–181, 1997.

[36] I. Bahar, A. Atilgan, M. Demirel, and B. Erman, “Vibrational Dynamics of Folded Proteins: Significance of Slow and Fast Motions in Relation to Function and Stability,” *Phys. Rev. Lett.*, vol. 80, no. 12, pp. 2733–2736, 1998.

[37] C. Micheletti, P. Carloni, and A. Maritan, “Accurate and Efficient Description of Protein Vibrational Dynamics: Comparing Molecular Dynamics and Gaussian Models,” *Proteins Struct. Funct. Genet.*, vol. 55, no. October 2003, pp. 635–645, 2004.

[38] K. Hamacher and J. a. McCammon, “Computing the amino acid specificity of fluctuations in biomolecular systems,” *J. Chem. Theory Comput.*, vol. 2, pp. 873–878, 2006.

[39] L. W. Yang and I. Bahar, “Coupling between catalytic site and collective dynamics: A requirement for mechanochemical activity of enzymes,” *Structure*, vol. 13, no. 6, pp. 893–904, 2005.

[40] N. Ozer, C. a Schiffer, and T. Haliloglu, “Rationale for more diverse inhibitors in competition with substrates in HIV-1 protease.,” *Biophys. J.*, vol. 99, no. 5, pp. 1650–9, Sep. 2010.

[41] W. Humphrey, A. Dalke, and K. Schulten, “{VMD} -- {V}isual {M}olecular {D}ynamics,” *J. Mol. Graph.*, vol. 14, pp. 33–38, 1996.

[42] J. A. McCammon, B. R. Gelin, and M. Karplus, “Dynamics of folded proteins,” *Nature*, vol. 267, pp. 585–590, 1977.

[43] W. D. Cornell, P. Cieplak, C. I. Bayly, I. R. Gould, K. M. Merz, D. M. Ferguson, D. C. Spellmeyer, T. Fox, J. W. Caldwell, and P. A. Kollman, “A second generation force field for the simulation of proteins, nucleic acids, and organic molecules,” *J Am Chem Soc*, vol. 117, pp. 5179–5197, 1995.

[44] J. C. Phillips, R. Braun, W. Wang, J. Gumbart, E. Tajkhorshid, E. Villa, C. Chipot, R. D. Skeel, L. Kalé, and K. Schulten, “Scalable molecular dynamics with NAMD,” *J. Comput. Chem.*, vol. 26, pp. 1781–1802, 2005.

[45] MacKerell A. D., D. Bashford, M. Bellott, Dunbrack R. L., J. D. Evanseck, M. J. Field, S. Fischer, J. Gao, H. Guo, S. Ha, D. Joseph-McCarthy, L. Kuchnir, K. Kuczera, F. T. K. Lau, C. Mattos, S. Michnick, T. Ngo, D. T. Nguyen, B. Prodhom, W. E. Reiher, B. Roux, M. Schlenkrich, J. C. Smith, R. Stote, J. Straub, M. Watanabe, J. Wiórkiewicz-Kuczera, D. Yin, and M. Karplus, “All-Atom Empirical Potential for Molecular Modeling and Dynamics Studies of Proteins,” *J. Phys. Chem. B*, vol. 102, no. 18, pp. 3586–3616, Apr. 1998.

[46] M. Feig, J. Karanicolas, and C. L. Brooks, “MMTSB Tool Set: Enhanced sampling and multiscale modeling methods for applications in structural biology,” *J. Mol. Graph. Model.*, vol. 22, pp. 377–395, 2004.

[47] N. Özer, A. Özen, C. a. Schiffer, and T. Haliloğlu, “Drug-resistant HIV-1 protease regains functional dynamics through cleavage site coevolution,” *Evol. Appl.*, vol. 8, no. 2, pp. 185–198, 2015.

[48] E. Lyman and D. M. Zuckerman, “Ensemble-based convergence analysis of biomolecular trajectories.,” *Biophys. J.*, vol. 91, no. July, pp. 164–172, 2006.

[49] a. J. Rader, D. H. Vlad, and I. Bahar, “Maturation dynamics of bacteriophage HK97 capsid,” *Structure*, vol. 13, no. 3, pp. 413–421, 2005.

[50] J.-H. Min, H. Yang, M. Ivan, F. Gertler, W. G. Kaelin, and N. P. Pavletich, “Structure of an HIF-1alpha -pVHL complex: hydroxyproline recognition in signaling.,” *Science*, vol. 296, no. June, pp. 1886–1889, 2002.

AUTOBIOGRAPHY

Name Surname **:** Tandaç Fürkan GÜÇLÜ

Place and Date of Birth **:** Trabzon/13.06.1989

Foreign Language **:** English

E-mail **:** tfguclu@gmail.com

Education

Degree	Department/Program	University/High School	GraduationYear
High School	Science	Kırklareli Science High School	2007
Bachelor of Science	Biology	Hacettepe University	2013

Poster Presentations in International Conferences:

T.F. Guclu, P. Ozbek, N. Ozer, "Comparative Study of Functional Dynamics in Mutant von Hippel-Lindau Tumor Suppressor Protein Structures", Biophysical Society Thematic Meeting "Modeling of Biomolecular Systems Interactions, Dynamics, and Allostery: Bridging Experiments and Computations", Istanbul, Turkey, 2014.

T.F. Guclu, P. Ozbek, N. Ozer, "Dynamic Analysis of Mutant von Hippel-Lindau Tumor Suppressor Protein Structures", 2nd International BAU Drug Design Congress, Istanbul, Turkey, 2014.